sufficient for cell cycle re-entry. *Nature* (2003) 424(6945):223-228.

34. SEBASTIAN T, MALIK R, THOMAS S, SAGE J, JOHNSON PF: C/EBPβ cooperates with RB:E2F to implement Ras(V12)-induced cellular senescence. *EMBO J.* (2005) 24(18):3301-3312.

35. CARR J, MACKIE RM: Point mutations in the N-ras oncogene in malignant melanoma and congenital naevi. *Br. J. Dermatol.* (1994) 131(1):72-77.

36. DAVIES H, BIGNELL GR, COX C *et al.*: Mutations of the BRAF gene in human cancer. *Nature* (2002) 417(6892):949-954.

37. POLLOCK PM, HARPER UL, HANSEN KS *et al.*: High frequency of BRAF mutations in nevi. *Nat. Genet.* (2003) 33(1):19-20.

• **Demonstration of clinical importance of oncogene-induced senescence in nevi.**

38. CHEN Z, TROTMAN LC, SHAFFER D *et al.*: Crucial role of p53-dependent cellular senescence in suppression of Pten-deficient tumorigenesis. *Nature* (2005) 436(7051):725-730.

39. LAZZERINI DENCHI E, ATTWOOLL C, PASINI D, HELIN K: Deregulated E2F activity induces hyperplasia and senescence-like features in the mouse pituitary gland. *Mol. Cell Biol.* (2005) 25(7):2660-2672.

40. GREENBERG RA, CHIN L, FEMINO A *et al.*: Short dysfunctional telomeres impair tumorigenesis in the INK4a(δ2/3) cancer-prone mouse. *Cell* (1999) 97(4):515-525.

41. FELDSER DM, GREIDER CW: Short telomeres limit tumor progression *in vivo* by inducing senescence. *Cancer Cell* (2007) 11(5):461-469.

42. COSME-BLANCO W, SHEN MF, LAZAR AJ *et al.*: Telomere dysfunction suppresses spontaneous tumorigenesis *in vivo* by initiating p53-dependent cellular senescence. *EMBO Rep.* (2007) 8(5):497-503.

43. XUE W, ZENDER L, MIETHING C *et al.*: Senescence and tumour clearance is triggered by p53 restoration in murine liver carcinomas. *Nature* (2007) 445(7128):656-660.

44. VENTURA A, KIRSCH DG, MCLAUGHLIN ME *et al.*: Restoration of p53 function leads to tumour regression *in vivo*. *Nature* (2007) 445(7128):661-665.

45. MARTINS CP, BROWN-SWIGART L, EVAN GI: Modeling the therapeutic efficacy of p53 restoration in tumors. *Cell* (2006) 127(7):1323-1334.

46. HAQ R, BRENTON JD, TAKAHASHI M *et al.*: Constitutive p38HOG mitogen-activated protein kinase activation induces permanent cell cycle arrest and senescence. *Cancer Res.* (2002) 62(17):5076-5082.

47. IWASA H, HAN J, ISHIKAWA F: Mitogen-activated protein kinase p38 defines the common senescence-signalling pathway. *Genes Cells* (2003) 8(2):131-144.

48. SUN P, YOSHIZUKA N, NEW L *et al.*: PRAK is essential for ras-induced senescence and tumor suppression. *Cell* (2007) 128(2):295-308.

49. ODA K, ARAKAWA H, TANAKA T *et al.*: p53AIP1, a potential mediator of p53-dependent apoptosis, and its regulation by Ser-46-phosphorylated p53. *Cell* (2000) 102(6):849-862.

50. BULAVIN DV, SAITO S, HOLLANDER MC *et al.*: Phosphorylation of human p53 by p38 kinase coordinates N-terminal phosphorylation and apoptosis in response to UV radiation. *EMBO J.* (1999) 18(23):6845-6854.

51. D'ORAZI G, CECCHINELLI B, BRUNO T *et al.*: Homeodomain-interacting protein kinase-2 phosphorylates p53 at Ser 46 and mediates apoptosis. *Nat. Cell Biol.* (2002) 4(1):11-19.

52. FERBEYRE G, DE STANCHINA E, QUERIDO E *et al.*: PML is induced by oncogenic ras and promotes premature senescence. *Genes Dev.* (2000) 14(16):2015-2027.

53. PEARSON M, CARBONE R, SEBASTIANI C *et al.*: PML regulates p53 acetylation and premature senescence induced by oncogenic Ras. *Nature* (2000) 406(6792):207-210.

54. BISCHOF O, KIRSH O, PEARSON M *et al.*: Deconstructing PML-induced premature senescence. *EMBO J.* (2002) 21(13):3358-3369.

55. SYKES SM, MELLERT HS, HOLBERT MA *et al.*: Acetylation of the p53 DNA-binding domain regulates apoptosis induction. *Mol. Cell* (2006) 24(6):841-851.

56. TANG Y, LUO J, ZHANG W, GU W: Tip60-dependent acetylation of p53 modulates the decision between cell-cycle arrest and apoptosis. *Mol. Cell* (2006) 24(6):827-839.

57. TYTECA S, VANDROMME M, LEGUBE G, CHEVILLARD-BRIET M, TROUCHE D: Tip60 and p400 are both required for UV-induced apoptosis but play antagonistic roles in cell cycle progression. *EMBO J.* (2006) 25(8):1680-1689.

58. LEGUBE G, LINARES LK, LEMERCIER C *et al.*: Tip60 is targeted to proteasome-mediated degradation by Mdm2 and accumulates after UV irradiation. *EMBO J.* (2002) 21(7):1704-1712.

59. SUN Y, JIANG X, CHEN S, FERNANDES N, PRICE BD: A role for the Tip60 histone acetyltransferase in the acetylation and activation of ATM. *Proc. Natl. Acad. Sci. USA* (2005) 102(37):13182-13187.

60. SQUATRITO M, GORRINI C, AMATI B: Tip60 in DNA damage response and growth control: many tricks in one HAT. *Trends Cell Biol.* (2006) 16(9):433-442.

61. PANTOJA C, SERRANO M: Murine fibroblasts lacking p21 undergo senescence and are resistant to transformation by oncogenic Ras. *Oncogene* (1999) 18(35):4974-4982.

62. HEROLD S, WANZEL M, BEUGER V *et al.*: Negative regulation of the mammalian UV response by Myc through association with Miz-1. *Mol. Cell* (2002) 10(3):509-521.

63. RANGARAJAN A, TALORA C, OKUYAMA R *et al.*: Notch signaling is a direct determinant of keratinocyte growth arrest and entry into differentiation. *EMBO J.* (2001) 20(13):3427-3436.

64. CARREIRA S, GOODALL J, AKSAN I *et al.*: Mitf cooperates with Rb1 and activates p21Cip1 expression to regulate cell cycle progression. *Nature* (2005) 433(7027):764-769.

65. DENG C, ZHANG P, HARPER JW, ELLEDGE SJ, LEDER P: Mice lacking p21CIP1/WAF1 undergo normal development, but are defective in G1 checkpoint control. *Cell* (1995) 82(4):675-684.

66. SEOANE J, LE HV, MASSAGUE J: Myc suppression of the p21(Cip1) Cdk inhibitor influences the outcome of the p53 response to DNA damage. *Nature* (2002) 419(6908):729-734.

67. WU S, CETINKAYA C, MUNOZ-ALONSO MJ *et al.*: Myc represses differentiation-induced p21CIP1 expression via Miz-1-dependent interaction with the p21 core promoter. *Oncogene* (2003) 22(3):351-360.

68. ZINDY F, EISCHEN CM, RANDLE DH *et al.*: Myc signaling via the ARF tumor suppressor regulates p53-dependent apoptosis and immortalization. *Genes Dev.* (1998) 12(15):2424-2433.

69. LU ZH, BOOKS JT, LEY TJ: YB-1 is important for late-stage embryonic development, optimal cellular stress responses, and the prevention of premature senescence. *Mol. Cell Biol.* (2005) 25(11):4625-4637.

70. SPARMANN A, VAN LOHUIZEN M: Polycomb silencers control cell fate, development and cancer. *Nat. Rev. Cancer* (2006) 6(11):846-856.

- **A comprehensive review on Polycomb group (PcG) proteins.**

71. BRACKEN AP, DIETRICH N, PASINI D, HANSEN KH, HELIN K: Genome-wide mapping of Polycomb target genes unravels their roles in cell fate transitions. *Genes Dev.* (2006) 20(9):1123-1136.

- **Description of global change in distribution of the Polycomb group (PcG) proteins on mammalian genome upon cell differentiation.**

72. BRACKEN AP, KLEINE-KOHLBRECHER D, DIETRICH N *et al.*: The Polycomb group proteins bind throughout the INK4A-ARF locus and are disassociated in senescent cells. *Genes Dev.* (2007) 21(5):525-530.

- **Demonstration of a mechanism how p16 is upregulated in senescent cells.**

73. YANNONI YM, GAESTEL M, LIN LL: P66(ShcA) interacts with MAPKAP kinase 2 and regulates its activity. *FEBS Lett.* (2004) 564(1-2):205-211.

74. VONCKEN JW, NIESSEN H, NEUFELD B *et al.*: MAPKAP kinase 3pK phosphorylates and regulates chromatin association of the polycomb group protein Bmi1. *J. Biol. Chem.* (2005) 280(7):5178-5187.

- **The first evidence that MK's are involved in regulation of the polycomb proteins binding to chromatin.**

75. GAESTEL M: MAPKAP kinases – MKs – two's company, three's a crowd. *Nat. Rev. Mol. Cell Biol.* (2006) 7(2):120-130.

- A comprehensive review on MK2, 3 and 5.

76. MANKE IA, NGUYEN A, LIM D *et al.*: MAPKAP kinase-2 is a cell cycle checkpoint kinase that regulates the G2/M transition and S phase progression in response to UV irradiation. *Mol. Cell* (2005) 17(1):37-48.

77. PASSEGUE E, WAGNER EF: JunB suppresses cell proliferation by transcriptional activation of p16(INK4a) expression. *EMBO J.* (2000) 19(12):2969-2979.

78. OHTANI N, ZEBEDEE Z, HUOT TJ *et al.*: Opposing effects of Ets and Id proteins on p16INK4a expression during cellular senescence. *Nature* (2001) 409(6823):1067-1070.

79. YEE AS, PAULSON EK, MCDEVITT MA *et al.*: The HBP1 transcriptional repressor and the p38 MAP kinase: unlikely partners in G1 regulation and tumor suppression. *Gene* (2004) 336(1):1-13.

80. ZHANG X, KIM J, RUTHAZER R *et al.*: The HBP1 transcriptional repressor participates in RAS-induced premature senescence. *Mol. Cell Biol.* (2006) 26(22):8252-8266.

81. VENTURA JJ, TENBAUM S, PERDIGUERO E *et al.*: p38α MAP kinase is essential in lung stem and progenitor cell proliferation and differentiation. *Nat. Genet.* (2007) 39(6):750-758.

82. VERSTEEGE I, SEVENET N, LANGE J *et al.*: Truncating mutations of hSNF5/INI1 in aggressive paediatric cancer. *Nature* (1998) 394(6689):203-206.

83. BIEGEL JA, ZHOU JY, RORKE LB *et al.*: Germ-line and acquired mutations of INI1 in atypical teratoid and rhabdoid tumors. *Cancer Res.* (1999) 59(1):74-79.

84. ROBERTS CW, GALUSHA SA, MCMENAMIN ME, FLETCHER CD, ORKIN SH: Haploinsufficiency of Snf5 (integrase interactor 1) predisposes to malignant rhabdoid tumors in mice. *Proc. Natl. Acad. Sci. USA* (2000) 97(25):13796-13800.

85. ROBERTS CW, LEROUX MM, FLEMING MD, ORKIN SH: Highly penetrant, rapid tumorigenesis through conditional inversion of the tumor suppressor gene Snf5. *Cancer Cell* (2002) 2(5):415-425.

86. CHAI J, CHARBONEAU AL, BETZ BL, WEISSMAN BE: Loss of the *hSNF5* gene concomitantly inactivates p21CIP/WAF1 and p16INK4a activity associated with replicative senescence in A204 rhabdoid tumor cells. *Cancer Res.* (2005) 65(22):10192-10198.

87. ORUETXEBARRIA I, VENTURINI F, KEKARAINEN T *et al.*: P16INK4a is required for hSNF5 chromatin remodeler-induced cellular senescence in malignant rhabdoid tumor cells. *J. Biol. Chem.* (2004) 279(5):3807-3816.

88. SCHUETTENGRUBER B, CHOURROUT D, VERVOORT M, LEBLANC B, CAVALLI G: Genome regulation by polycomb and trithorax proteins. *Cell* (2007) 128(4):735-745.

- **A comprehensive review on functions of the polycomb and trithorax group of proteins.**

89. NARITA M, NUNEZ S, HEARD E *et al.*: Rb-mediated heterochromatin formation and silencing of E2F target genes during cellular senescence. *Cell* (2003) 113(6):703-716.

- **Identification of SAHF formation as a maintenance mechanism of cellular senescence.**

90. ZHANG R, POUSTOVOITOV MV, YE X *et al.*: Formation of macroH2A-containing senescence-associated heterochromatin foci and senescence driven by ASF1a and HIRA. *Dev. Cell* (2005) 8(1):19-30.

91. NARITA M, NARITA M, KRIZHANOVSKY V *et al.*: A novel role for high-mobility group a proteins in cellular senescence and heterochromatin formation. *Cell* (2006) 126(3):503-514.

92. MITSUI Y, SAKAGAMI H, MUROTA S, YAMADA M: Age-related decline in histone H1 fraction in human diploid fibroblast cultures. *Exp. Cell Res.* (1980) 126(2):289-298.

93. ROGAKOU EP, SEKERI-PATARYAS KE: Histone variants of H2A and H3 families are regulated during *in vitro* aging in the same manner as during differentiation. *Exp. Gerontol.* (1999) 34(6):741-754.

94. FUNAYAMA R, SAITO M, TANOBE H, ISHIKAWA F: Loss of linker histone H1 in cellular senescence. *J. Cell Biol.* (2006) 175(6):869-880.

95. FUNAYAMA R, ISHIKAWA F: Cellular senescence and chromatin structure. *Chromosoma* (2007):(In Press).

- A comprehensive reviw on SAHF formation.

96. ZHANG R, CHEN W, ADAMS PD: Molecular dissection of formation of

senescence-associated heterochromatin foci. *Mol. Cell Biol.* (2007) 27(6):2343-2358.

97. BRAIG M, LEE S, LODDENKEMPER C *et al.*: Oncogene-induced senescence as an initial barrier in lymphoma development. *Nature* (2005) 436(7051):660-665.

98. RASTOGI S, JOSHI B, DASGUPTA P *et al.*: Prohibitin facilitates cellular senescence by recruiting specific corepressors to inhibit E2F target genes. *Mol. Cell Biol.* (2006) 26(11):4161-4171.

99. KIYONO T, FOSTER SA, KOOP JI *et al.*: Both Rb/p16INK4a inactivation and telomerase activity are required to immortalize human epithelial cells. *Nature* (1998) 396(6706):84-88.

100. JARRARD DF, SARKAR S, SHI Y *et al.*: p16/pRb pathway alterations are required for bypassing senescence in human prostate epithelial cells. *Cancer Res.* (1999) 59(12):2957-2964.

101. ITAHANA K, ZOU Y, ITAHANA Y *et al.*: Control of the replicative life span of human fibroblasts by p16 and the polycomb protein Bmi-1. *Mol. Cell Biol.* (2003) 23(1):389-401.

102. HAGA K, OHNO S, YUGAWA T *et al.*: Efficient immortalization of primary human cells by p16INK4a-specific short hairpin RNA or Bmi-1, combined with introduction of hTERT. *Cancer Sci.* (2007) 98(2):147-154.

103. RAMIREZ RD, SHERIDAN S, GIRARD L *et al.*: Immortalization of human bronchial epithelial cells in the absence of viral oncoproteins. *Cancer Res.* (2004) 64(24):9027-9034.

104. JACOBS JJ, KIEBOOM K, MARINO S, DEPINHO RA, VAN LOHUIZEN M: The oncogene and polycomb-group gene Bmi-1 regulates cell proliferation and senescence through the INK4a locus. *Nature* (1999) 397(6715):164-168.

• **Establishing a link between the polycomb group protein, transcriptional repression of the INK4A locus and senescence.**

105. GIL J, BERNARD D, MARTINEZ D, BEACH D: Polycomb CBX7 has a unifying role in cellular lifespan. *Nat. Cell Biol.* (2004) 6(1):67-72.

106. DIETRICH N, BRACKEN AP, TRINH E *et al.*: Bypass of senescence by the polycomb group protein CBX8 through direct binding to the INK4A-ARF locus. *EMBO J.* (2007) 26(6):1637-1648.

107. MARTIN GM: Genetic modulation of senescent phenotypes in *Homo sapiens*. *Cell* (2005) 120(4):523-532.

• **A comprehensive review on human progeria syndromes and ageing.**

108. RAMIREZ RD, MORALES CP, HERBERT BS *et al.*: Putative telomere-independent mechanisms of replicative aging reflect inadequate growth conditions. *Genes Dev.* (2001) 15(4):398-403.

109. HERBERT BS, WRIGHT WE, SHAY JW: p16(INK4a) inactivation is not required to immortalize human mammary epithelial cells. *Oncogene* (2002) 21(51):7897-7900.

110. ZINDY F, QUELLE DE, ROUSSEL MF, SHERR CJ: Expression of the p16INK4a tumor suppressor versus other INK4 family members during mouse development and aging. *Oncogene* (1997) 15(2):203-211.

111. NIELSEN GP, STEMMER-RACHAMIMOV AO, SHAW J *et al.*: Immunohistochemical survey of p16INK4A expression in normal human adult and infant tissues. *Lab. Invest.* (1999) 79(9):1137-1143.

112. NYSTUL TG, SPRADLING AC: Breaking out of the mold: diversity within adult stem cells and their niches. *Curr. Opin. Genet. Dev.* (2006) 16(5):463-468.

113. ITO M, YANG Z, ANDL T *et al.*: Wnt-dependent de novo hair follicle regeneration in adult mouse skin after wounding. *Nature* (2007) 447(7142):316-320.

114. WATKINS DN, BERMAN DM, BURKHOLDER SG *et al.*: Hedgehog signalling within airway epithelial progenitors and in small-cell lung cancer. *Nature* (2003) 422(6929):313-317.

115. BEACHY PA, KARHADKAR SS, BERMAN DM: Tissue repair and stem cell renewal in carcinogenesis. *Nature* (2004) 432(7015):324-331.

116. WATKINS DN, PEACOCK CD: Hedgehog signalling in foregut malignancy. *Biochem. Pharmacol.* (2004) 68(6):1055-1060.

117. PEACOCK CD, WANG Q, GESELL GS *et al.*: Hedgehog signaling maintains a tumor stem cell compartment in multiple myeloma. *Proc. Natl. Acad. Sci. USA* (2007) 104(10):4048-4053.

118. STECCA B, MAS C, CLEMENT V *et al.*: Melanomas require HEDGEHOG-GLI signaling regulated by interactions between GLI1 and the RAS-MEK/AKT pathways. *Proc. Natl. Acad. Sci. USA* (2007) 104(14):5895-5900.

119. ATHAR M, TANG X, LEE JL, KOPELOVICH L, KIM AL: Hedgehog signalling in skin development and cancer. *Exp. Dermatol.* (2006) 15(9):667-677.

120. RADTKE F, CLEVERS H, RICCIO O: From gut homeostasis to cancer. *Curr. Mol. Med.* (2006) 6(3):275-289.

121. AKIYOSHI T, NAKAMURA M, KOGA K *et al.*: Gli1, downregulated in colorectal cancers, inhibits proliferation of colon cancer cells involving Wnt signalling activation. *Gut* (2006) 55(7):991-999.

122. SENGUPTA A, BANERJEE D, CHANDRA S *et al.*: Deregulation and cross talk among Sonic hedgehog, Wnt, Hox and Notch signaling in chronic myeloid leukemia progression. *Leukemia* (2007) 21(5):949-955.

123. KMITA M, TARCHINI B, ZAKANY J *et al.*: Early developmental arrest of mammalian limbs lacking HoxA/HoxD gene function. *Nature* (2005) 435(7045):1113-1116.

124. PRASAD NB, BIANKIN AV, FUKUSHIMA N *et al.*: Gene expression profiles in pancreatic intraepithelial neoplasia reflect the effects of Hedgehog signaling on pancreatic ductal epithelial cells. *Cancer Res.* (2005) 65(5):1619-1626.

125. GIL J, KERAI P, LLEONART M *et al.*: Immortalization of primary human prostate epithelial cells by c-Myc. *Cancer Res.* (2005) 65(6):2179-2185.

126. GILES RH, VAN ES JH, CLEVERS H: Caught up in a Wnt storm: Wnt signaling in cancer. *Biochim. Biophys. Acta* (2003) 1653(1):1-24.

127. SANSOM OJ, MENIEL VS, MUNCAN V *et al.*: Myc deletion rescues Apc deficiency in the small intestine. *Nature* (2007) 446(7136):676-679.

Affiliation

Tohru Kiyono
National Cancer Center Research Institute,
Virology Division,
5-1-1 Tsukiji, Chuo-ku,
Tokyo 104-0045, Japan
Tel: +81 3 3547 5275; Fax: +81 3 3543 2181;
E-mail: tkiyono@gan2.res.ncc.go.jp

Cell Tissue Res (2008) 331:461–472
DOI 10.1007/s00441-007-0528-x

REGULAR ARTICLE

Characteristic phenotype of immortalized periodontal cells isolated from a Marfan syndrome type I patient

Momotoshi Shiga · Masahiro Saito · Mitsu Hattori · Chiharu Torii · Kenjiro Kosaki · Tohru Kiyono · Naoto Suda

Received: 17 May 2007 / Accepted: 20 September 2007 / Published online: 30 November 2007

Abstract The periodontal ligament (PDL) is situated between the tooth root and alveolar bone, thereby supporting the tooth, and is composed of collagen and elastic system fibers. Marfan syndrome type I (MFS1, MIM #154700) is caused by mutations in *FBN1* encoding fibrillin-1, which is a major microfibrillar protein of elastic system fibers. MFS1 is characterized by tall stature, aortic/mitral valve prolapse, and ectopia lentis and is occasionally accompanied by severe periodontitis. Since little is known about the biological functions of elastic system fibers in PDLs and the pathogenesis of the periodontitis in MFS1, PDL cells were isolated from an MFS1 patient with a heterozygous missense mutation in a calcium-binding epidermal-growth-factor-like domain of *FBN1*. Isolated PDL cells were immortalized by transducing a retrovirus carrying genes for the human Polycomb group protein, Bmi-1, and human telomerase reverse transcriptase. Immortalized PDL cells from the MFS1 patient (termed M-HPL1) and those of a healthy volunteer (termed HPDL2) both expressed various PDL-related genes. The growth and attachment of M-HPL1 and HPDL2 to hydroxyapatite particles were comparable. However, when M-HPL1 were transplanted with hydroxyapatite particles into immunodeficient mice, disorganized cell alignment and irregular microfibril assembly were noted. The activation of the signaling of transforming grwoth factor-β (TGF-β) is thought to cause the pathogenesis for lung and cardiovascular abnormalities in MFS1. Interestingly, M-HPL1 shows a higher level of activated TGF-β than HPDL2. Thus, M-HPL1 represent a powerful tool for clarifying the biological roles of elastic system fibers in PDL and the pathogenesis of periodontitis in MFS1. Our findings also suggest that *FBN1* regulates cell alignment and microfibril assembly in PDLs.

Keywords Elastic fiber · Fibrillin-1 · Marfan syndrome · Periodontitis · Periodontal ligament · Human

This work was supported by Grants-in-Aid (16390604, 16659570, and 18390552) for Scientific Research from the Ministry of Education, Culture, Sports, Science, and Technology of Japan.

M. Shiga · M. Hattori · N. Suda (✉)
Maxillofacial Orthognathics, Department of Maxillofacial Reconstruction and Function,
Division of Maxillofacial/Neck Reconstruction, Graduate School,
Tokyo Medical and Dental University,
1-5-45 Yushima, Bunkyo-ku,
Tokyo 113-8549, Japan
e-mail: n-suda.mort@tmd.ac.jp

M. Saito
Department of Molecular and Cellular Biochemistry,
Graduate School of Dentistry, Osaka University,
Osaka 565-0871, Japan

C. Torii · K. Kosaki
Department of Pediatrics, Keio University School of Medicine,
Tokyo 160-8582, Japan

T. Kiyono
Virology Division, National Cancer Center Research Institute,
Tokyo 104-0045, Japan

Introduction

The periodontal ligament (PDL) is a specialized connective tissue situated between the cementum covering the root of teeth and the alveolar bone socket (Beertsen et al. 1997; Freeman 1998). PDLs consist of various kinds of cells and fibers. The cells include fibroblasts, epithelial cell remnants of Malassez, macrophages, undifferentiated mesenchymal cells, cementoblasts, osteoblasts, and osteoclasts. The fibers include collagen and elastic system fibers. PDLs are well adapted to support teeth in bone and to act as a sensory

receptor. To support teeth, collagen fibers are embedded both in the cementum and alveolar bone, and each collagen fiber works as a spliced rope to withstand the considerable forces of mastication.

Elastic system fibers provide elasticity and resistance to stretch and expansion forces (Mecham 1991). They are widely distributed in various tissues, e.g., skin, lungs, eyes, and blood vessels. Three types of elastic system fibers (oxytalan and elastic and elaunin fibers) are known; they differ in the content of elastin (Kielty et al. 2002). Oxytalan fibers solely consist of bundles of microfibrils, which are predominantly composed of glycoproteins and fibrillin-1 and -2. The elastic fibers are constructed of bundles of microfibrils peripherally associated with elastin. In the elaunin fibers, bundles of microfibrils are intermingled with small amounts of elastin. In the PDL, the main elastic system fibers are oxytalan fibers oriented in an occluso-apical direction (Fullmer et al. 1974; Beertsen et al. 1997). A small amount of elaunin fibers is also found in the apical region (Staszyk and Gasse 2004; Sawada et al. 2006). In contrast to collagen fibers, the biological functions of the elastic system fibers in PDLs are still obscure.

Marfan syndrome type I (MFS1, MIM #154700) is an autosomal dominant disorder affecting the elastic system fibers. Its prevalence has been estimated to be 2–3 per 10,000 (Nollen and Mulder 2004). MFS1 is characterized by various clinical manifestations primarily in skeletal, ocular, and cardiovascular organs, e.g., tall stature, aortic dissection, mitral valve prolapse, and ectopia lentis (Pyeritz 2000). The responsible gene for this syndrome has been identified as *FBN1*, which encodes the major microfibrillar protein, fibrillin-1 (Dietz et al. 1991; Maslen et al. 1991). In addition to anomalies in skeletal, ocular, and cardiovascular systems, MFS1 exhibits characteristic oral features including maxillary protrusion (Westling et al. 1998), high palate, and crowding and fragility of the temporomandibular joint (Bauss et al. 2004). Severe periodontitis, which has a serious impact on the quality of life of MFS1 patients, is occasionally associated with this syndrome (Straub et al. 2002).

To clarify the biological functions of fibrillin-1 in PDLs and the pathogenesis of the periodontitis in MFS1, PDL cells have been isolated from an MFS1 patient. The prepared immortalized PDL cells, which have a mutation in a calcium-binding epidermal-growth-factor-like (cbEGF) domain of fibrillin-1, might be a powerful tool to help answer these questions.

Materials and methods

Subjects

The patient was a 46-year-old female. She was 172 cm tall, weighed 58 kg, and had arachnodactyly. Her father and younger brother were also diagnosed as having Marfan syndrome. She had previously had dissecting aneurysm of the aorta and had had a surgical replacement of the aortic root (Bentall operation) at 42 years of age. She had suffered from mitral valve prolapse and had had a replacement of the mitral valve at 46 years of age. Since she had severe periodontitis in all teeth, all teeth were extracted before the mitral valve replacement to avoid infective endocarditis. The patient kindly provided these teeth to us with consent.

Extracted teeth were also provided by three healthy volunteers (volunteer A, 15-year-old male; volunteer B, 15-year-old male; volunteer C, 21-year-old female) during the course of orthodontic treatment, with consent. The experimental protocol was approved by the Ethical Review Committee of Tokyo Medical and Dental University.

Isolation and culture of primary PDL cells

Isolation and culture of human PDL cells were performed as previously described (Kapila et al. 1996; Shiga et al. 2003). In brief, the extracted teeth from the MFS1 patient and healthy volunteers were washed with α-minimum essential medium (α–MEM; Kohojin Bio, Japan) containing Antibiotic-Antimycotic (GIBCO, Calif.). The PDL attached to the middle part of the root was isolated with a surgical scalpel. The PDL was minced and placed in 35-mm tissue culture dishes (SUMILON, Japan). The explants were then covered with sterile glass coverslips and incubated in α–MEM with 10% fetal bovine serum (FBS; Japan Bioserum, Japan) at 37°C under 5% CO_2 and 95% air until cells outgrew from the explants. After the outgrowth of cells, coverslips were removed from the culture dishes. The culture medium was changed every 3 days. PDL cells from passages 3–7 were used for examing mineralization, measuring alkaline phosphatase (ALP) activity, and transduction.

Mineralization of the primary culture of PDL cells

To determine the mineralization of cultured PDL cells, cells were plated at 2.0×10^4 cells/cm^2 and cultured in α–MEM containing 10% FBS. After cells became confluent, the medium was changed to α–MEM containing 10% FBS with 50 μg/ml ascorbic acid (Wako, Japan), 10 nM dexamethasone (Sigma, Mo.), and 10 mM β-glycerophosphate (Sigma) in some cultures, as previously described (Cho et al. 1992; Nohutcu et al. 1997; Chien et al. 1999). The medium was changed every 3 days, and the cells were cultured for 3 weeks. Mineralized matrix in the culture were stained by Alizarin Red S (Wako, Japan) at the end of the culture (Saito et al. 2002). All experiments were performed in triplicate wells.

ALP activity

Cells were cultured under the same conditions as described above for mineralization. ALP activity was assayed in cell lysates by enzymatic conversion of the p-nitrophenylphosphate substrate to p-nitrophenol by using the LabAssay ALP kit (Wako) according to the manufacturer's instructions. The activity was recorded as millimoles per milligram per 15 min. The total protein amount in the cell lysates was measured by using the Bradford microassay (Bio-Rad, Calif.) according to the manufacturer's instructions.

Immunohistochemical staining of cultured PDL cells

Cultured PDL cells were immunohistochemically stained by using anti-human periostin rabbit polyclonal antibody (BioVendor laboratory Medicine, N.C.), anti-bovine collagen type XII monoclonal antibody (Clone 378D5, Kamiya Biomedical, Wash.), anti-active transforming growth factor-β (TGF-β) rabbit polyclonal antibody (LC1-30, provided by K. Flanders, National Cancer Institute, Md.; Flanders et al. 1989), or anti-human latency-associated peptide-β1 (LAP-β1) goat polyclonal antibody (R&D systems, Minn.). Cells (2.0×10^4 cells/cm^2) were cultured on poly-L-lysine-coated glass (Iwaki, Japan). They were then fixed with 4% paraformaldehyde (PFA) for 30 min, blocked with 1% bovine serum albumin (BSA), and incubated with each antibody for 1 h. Sections were then treated with Alexa Fluor 594 goat anti-rabbit IG (H+L; Invitrogen, Calif.), Alexa Fluor 488 goat anti-mouse IG (H+L; Invitrogen), or Alexa Fluor 488 donkey anti-goat IG (H+L; Invitrogen). As negative controls, primary antibodies were replaced with normal rabbit serum (Vector Laboratories, Calif.), mouse IgG (Jackson Immuno Research Laboratories, Pa.), or normal goat serum (Vector Laboratories). After washes with phosphate-buffered saline, fluorescence was observed by means of a fluorescence microscope (AF6000, Leica, Germany).

Mutational analysis

DNA from the MFS1 patient and healthy volunteers was extracted by using a DNA extraction kit (Bio-Rad, Calif.). Extracted DNA was amplified by using specific primers for *FBN1* and *TGFBR2* (encoding TGF-β receptor II, which is the responsible gene for Marfan syndrome type II; MFS2, MIM #154705; Mizuguchi et al. 2004). Primer sequences and polymerase chain reaction (PCR) conditions were as given on the website of "Multiple Malformation Syndromes (http://www.dhplc.jp/genetics/frame.html)" provided by the Department of Pediatrics, Division of Medical Genetics, Keio University School of Medicine. Mutations in each amplicon were analyzed by denaturing high-performance liquid chromatography (DHPLC), as described in previous studies (Kosaki et al. 2005; Udaka et al. 2005).

After DHPLC analysis, PCR products were purified on a desalting column and were sequenced by a dideoxy-sequencing method (BigDye Dideoxy sequencing kit, Applied BioSystems, Calif.) and an automated sequencer (ABI3100, Applied Biosystems; Udaka et al. 2005).

Retroviral vectors and infection

Primary PDL cells, obtained from a healthy volunteer and the MFS1 patient, were transduced with genes for human Polycomb group protein, Bmi-1, and human telomerase reverse transcriptase (hTERT) by using retrovirus-mediated gene transfer. The production and infection of LXSN-Bmi-1 and MSCVpuro-hTERT retroviruses were performed as described previously (Kyo et al. 2003; Saito et al. 2005). The infected cells were selected in the presence of geneticin (125 μg/ml) or puromycin (0.5 μg/ml). For combined retroviral infection, cells were sequentially transduced with LXSN-Bmi-1 and then with MSCVpuro-hTERT. Stably transduced cells were maintained in the medium described above.

Detection of telomerase activity

After infection, telomerase activity was determined by a telomerase repeat amplification assay by using the TRA-Peze Telomerase Detection Kit (CHEMICON International, Calif.), according to the manufacturer's instructions.

Cell proliferation in monolayer culture

To examine cell proliferation, cells were inoculated at 5.0×10^3 cells/cm^2 into 6-well dishes (Iwaki, Japan) and cultured in α–MEM containing 10% FBS. The medium was changed every 3 days, and cells were counted every 3 days up to day 15. All experiments were performed in triplicate wells.

Western blot analysis

The introduction of Bmi-1 was identified by Western blot analysis by using anti-human Bmi-1 monoclonal antibody (BD Pharmingen, San Diego, Calif.). Cells were cultured in α–MEM containing 10% FBS and lysed in buffer containing 50 mM TRIS-HCl (pH 7.4), 125 mM NaCl, 0.1% Nonident P-40 (NP-40; Sigma), and 1 mM each of EDTA and phenylmethylsulfonyl fluoride, followed by sonication. After electrophoretic resolution of the cell lysate (20 μg each protein) on 12.5% SDS-polyacrylamide gels, the proteins were transferred to polyvinylidene difluoride (PVDF) membranes (Amersham, N.J.). The subsequent

detection procedure was performed as described previously (Saito et al. 2005).

RNA preparation and reverse transcription/PCR

Total RNA was isolated from primary PDL cells (both from healthy volunteer B and the MFS1 patient) and from immortalized PDL cells cultured in α–MEM containing 10% FBS, by using ISOGEN (Nippon Gene, Japan) according to the manufacturer's instructions. cDNA was synthesized from 1 μg total RNA by QuantiTect Reverse Transcription (QIAGEN, Germany), and each cDNA was used as the template for subsequent PCR amplification. Amplification was performed in a GeneAmp PCR System 9700 (Applied Biosystems). The reaction conditions were 94°C for 1 min, 60°C for 30 s, and 72°C for 30 s. The sequences of the used primers were: *POSTN* encoding periostin, sense 5′-ATTGATGGAGTGCCTGTG-3′, antisense 5′-CCTTGGTGACCTCTTCTTG-3′; *ASPN* encoding asporin, sense 5′-CGATACAAAGAACTACAAAGGCT GG-3′, antisense 5′-GCATTTCCCAGTATTTCA CCG-3′; *COL12A1* encoding collagen type XII, sense 5′-CGGA CAGAGCCTTA CGTGCC-3′, antisense 5′-CTGCCC GGGTCCGTGG-3′; *BGLAP* encoding osteoclacin, sense 5′-CCTTTGTGTCCAAGCAGGAG-3′, antisense 5′-TCA GCCAACTCGTCACAGTC-3′; *OPN* encoding osteopontin, sense 5′-TTGCAGTGATTTGCTTTTGC-3′, antisense 5′-TGTGGGG CTAGGAGATTCTG-3′; *BSP* encoding bone sialoprotein, sense 5′-GAACCACTTCCCCACCT TTT-3′, antisense 5′-TCTGACCATCATAGCCATCG-3′; *COL1A1* encoding collagen type I, sense 5′-CTGACCTT CCTGCGCCTGATGTCC-3′, antisense 5′-GTCTGGGGC ACCAACGTCCAAGGG -3′; and a human gene encoding β-actin, sense 5′-ATGAGGATCCTCACCGAGCGCGGCT ACAG C-3′, antisense 5′-ACACCACTGTGTTGGCGTAC AGGTCTTTGC-3′. Optimization of PCR cycle number to allow semi-quantitative analysis was performed by generating saturation curves of amplified product against cycle number. Saturation was seen with 33, 34, 31, 34, 41, 41, 25, and 25 cycles for *POSTN*, *ASPN*, *COL12A1*, *BGLAP*, *OPN*, *BSP*, *COL1A*, and β-actin, respectively. Thus, the semi-quantitative gene expression analysis by reverse transcription/PCR (RT-PCR) was performed with 30, 31, 28, 31, 39, 39, 23, and 23 cycles for *POSTN*, *ASPN*, *COL12A1*, *BGLAP*, *OPN*, *BSP*, *COL1A*, and β-actin, respectively.

A 151-bp fragment of *POSTN* (2220–2370 in NM_006475), a 292-bp fragment of *ASPN* (1031–1322 in NM_017680) (Yamada et al. 2001), a 180-bp fragment of *COL12A1* (7041–7220 in NM_080645), a 151-bp fragment of *BGLAP* (122–272 in NM_199173), a 166-bp fragment of *OPN* (173–338 in NM_001040058), a 201-bp fragment of *BSP* (876–1076 in NM_004967), a 300-bp fragment of *COL1A1* (4180–4479 in NM_000088), and a 327-bp fragment of the gene encoding β-actin (641–967 in NM_001101) were separated on 2% agarose gels (Nippon Gene, Japan) by electrophoresis. The gels were stained with ethidium bromide, photographed under ultraviolet excitation, and analyzed by using picture-imaging software (Scion Image, Scion, Md.).

Cell adhesion assay

To examine the adhesion of PDL cells, viz., HPDL2 from healthy volunteer 2 and M-HPL1 from the MFS1 patient, to hydroxyapatite particles (size 300–500 μm; OSferion, Olympus, Japan), both types of cells were labeled by using the PKH26 Red Fluorescent Cell Linker Mini Kit (Sigma) and incubated with hydroxyapatite particles for 18 h in α–MEM containing 10% FBS. The attached cells were observed by using a fluorescence microscope (AF6000, Leica, Germany).

In vivo differentiation assay

Fiber formation in the HPDL2 and M-HPL1 cells was assessed as described previously (Handa et al. 2002; Saito et al. 2005; Yokoi et al. 2007). Briefly, 1.5×10^6 cells were incubated with 40 mg hydroxyapatite particles and fibrin clot (mixture of mouse fibrinogen and thrombin; Sigma). They were transplanted subcutaneously into 5-week-old male CB-17 *SCID/SCID* mice (Nihon Crea, Japan). Mice were sacrificed after 4 weeks and implanted tissues were collected. Three transplants were prepared for each group, and experiments were repeated in triplicate.

To examine human (not mouse) vimentin-positive cells in transplanted tissues, tissues were fixed in 4% PFA for 1 day, decalcified with 10% formic acid for 3 days, and embedded in paraffin, and 5-μm-thick sections were prepared. To avoid non-specific staining by mouse monoclonal antibodies, sections were blocked by using the M.O.M. kit (Vector Laboratories, Calif.) as previously described (Handa et al. 2002). Sections were incubated, for 1 h, with anti-human vimentin monoclonal antibody (V9, DAKO, Calif.), which recognizes human but not mouse cells. After being washed, sections were incubated with biotinylated secondary antibody (M.O.M. kit) and avidin-peroxidase conjugate (M.O.M. kit). The reaction was visualized by using diaminobenzidine.

To examine human fibrillin-1-positive cells, transplanted tissues were embedded in carboxymethyl cellulose compound (Finetec, Japan), and 5-μm-thick frozen sections were prepared (Kawamoto and Shimizu 2000). Frozen sections were incubated with anti-human fibrillin-1 rabbit polyclonal antibody (Elastin Products, Mo.) for 1 h. After being washed, sections were incubated with Alexa Fluor 594 goat anti-rabbit IG (H+L; Invitrogen), and fluorescence

was observed with a fluorescence microscope (AF6000, Leica, Germany).

Statistical analysis

Student's *t*-test was used to analyze differences in cell numbers between M-HPL1 and HPDL2. Each difference was considered significant at a *P*-value of less than 0.05.

Results

MFS1 patient with a heterozygous mutation in cbEGF domain of FBN1

As shown in Fig. 1a–d, the 46-year-old female patient had severe periodontitis. All teeth had to be extracted before the surgical replacement of the mitral valve to avoid infective endocarditis. Mutational analysis of *FBN1* and *TGFBR2* was performed by using a genomic DNA sample. Since *FBN1* and *TGFBR2* have 65 and 7 exons, respectively, screening of gene mutations before direct sequencing was performed by DHPLC. In total, 65 and 8 amplicons of *FBN1* and *TGFBR2*, respectively, were amplified by PCR and subsequently analyzed by DHPLC. Among them, the peak in the amplicon of exon 52 in *FBN1* from the MFS1 patient shifted to the left compared with that of the wild-type sample (Fig. 1e). This demonstrated heteroduplex formation of the amplicon from the MFS1 patient. Direct sequencing of this product was performed (Fig. 1f). A heterozygous mutation (A to G) was seen at position 6431 (from the translation site in NM_000138). This missense mutation resulted in the replacement of Asn by Ser at amino acid position 2144 (N2144S) in the 32th cbEGF domain (Fig. 1g; see also in previous study of this MFS1 patient in Hewett et al. 1993). Thus, this is not a single nucleotide polymorphism (SNP) or a novel mutation. The elution profile of DHPLC for *TGFBR2* did not show differences between the wild-type sample and MFS1 patient.

Phenotype of primary PDL cells with N2144S mutation from MFS1 patient

Cells were isolated from the PDL of extracted teeth from the MFS1 patient and were cultured in vitro. In order to examine the cellular phenotype of these isolated PDL cells, ALP activity (Fig. 2a) and mineralization (Fig. 2b) were examined. In the cell differentiation medium containing

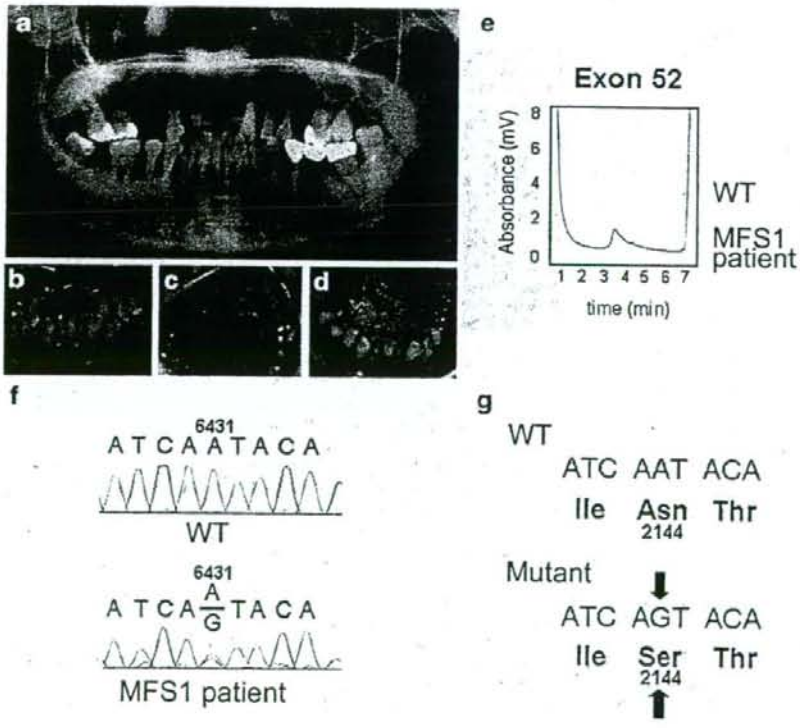

Fig. 1 Severe periodontitis and mutational analysis of the MFS1 patient. **a** In the panoramic X-ray, severe alveolar bone loss was observed around tooth roots. **b–d** Oral photographs showing the severe periodontitis of the patient. **e** DHPLC analysis of exon 52 in *FBN1*. Note the peak in the elution profile of the MFS1 patient shifted to the left compared with that of the wild-type (WT), demonstrating heteroduplex formation. **f** Nucleotide sequence of exon 52 in *FBN1*. **g** Amino acid sequence of fibrillin-1. The 6431A→G change resulted in the heterozygous missense mutation of Asn to Ser (N2144S)

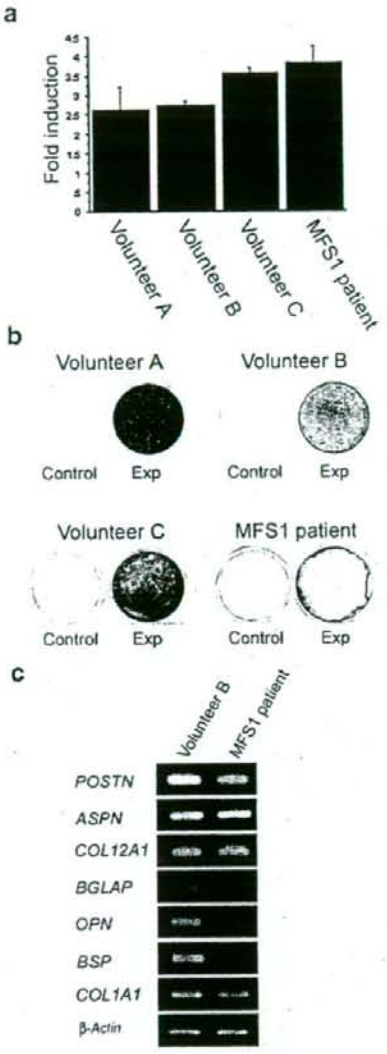

Fig. 2 **a** ALP activities of primary PDL cells isolated from three healthy volunteers (*volunteers A–C*) and the *MFS1 patient*. PDL cells were cultured in the cell differentiation medium containing ascorbic acid (50 μg/ml), β-glycerophosphate (10 mM), and dexamethasone (10 nM) for 3 weeks. Each ALP activity is represented as the ratio (*Fold induction*) to the value before culturing in the cell differentiation medium. PDL cells isolated from the MFS1 patient showed increased ALP activity as in healthy volunteers. **b** Mineralization of PDL cells cultured in the cell differentiation medium for 3 weeks. All PDL cells cultured in the cell differentiation medium were stained positively with Alizarin Red (*Exp*), but were negative when cultured in the medium containing 10% FBS solely (*Control*). **c** Expression of PDL-related genes, such as *POSTN* encoding periostin, *ASPN* encoding asporin, *COL12A1* encoding collagen type XII, *BGLAP* encoding osteocalcin, *OPN* encoding osteopontin, *BSP* encoding bone sialoprotein, *COL1A1* encoding collagen type I, and a human gene encoding β-actin, in cells from volunteer B and the MFS1 patient; reverse transcription/polymerase chain reaction (RT-PCR)

β-glycerophosphate, dexamethasone and ascorbic acid, these cells showed increased ALP activity, as did PDL cells of healthy volunteers (volunteers A–C) after a 3-week culture (Fig. 2a). The PDL cells from the MFS1 patient and healthy volunteers showed mineralization in the cell differentiation medium, but not in the medium only containing 10% FBS (Fig. 2b). The levels of the mineralization varied among cultures. Based on the similarities in the level of mineralization, PDL cells from volunteer B and MFS1 patient were selected for use in the further experiments.

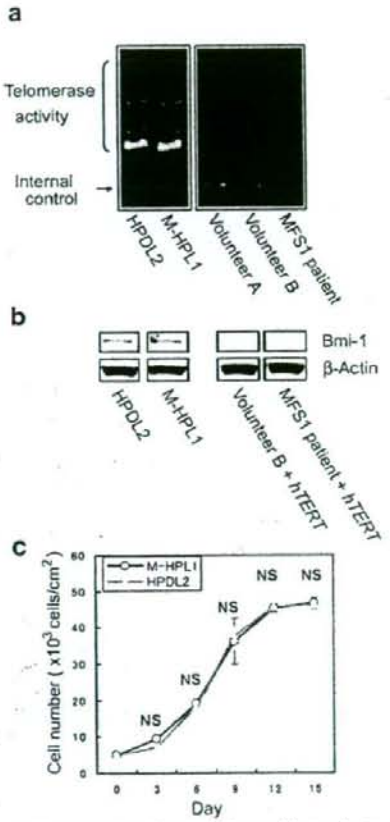

Fig. 3 **a**, **b** Telomerase activity and Western blot analysis of Bmi-1, respectively, in *hTERT*- and *Bmi-1*-transfected HPDL2 (originally from healthy volunteer B) and M-HPL1 (originally from the MFS1 patient). Note the characteristic ladder formation showing telomerase activity in HPDL2 and M-HPL1, but not in untransfected cells (volunteers A or B or MFS1 patient). Western blot analysis showing the expression of Bmi-1 in HPDL2 and M-HPL1, but not in cells transfected solely with *hTERT* (*Volunteer B + hTERT, MFS1 patient + hTERT*). **c** Proliferation of HPDL2 and M-HPL1 in culture. No significant difference occurs in the growth of the two types of cells at days 3, 6, 9, 12, 15 (*NS* not significant). Data represent means ± SD (n=3)

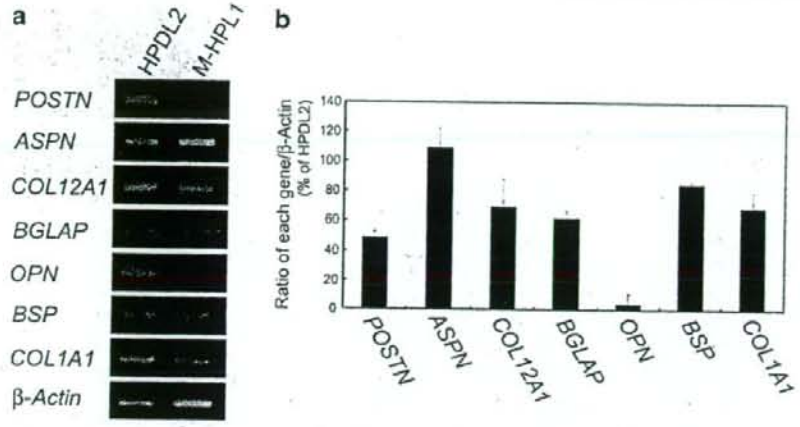

Fig. 4 **a** Expression of *POSTN* encoding periostin, *ASPN* encoding asporin, *COL12A1* encoding collagen type XII, *BGLAP* encoding osteocalcin, *OPN* encoding osteopontin, *BSP* encoding bone sialoprotein, *COL1A1* encoding collagen type I, and a human gene encoding β-actin in immortalized HPDL2 and M-HPL1; RT-PCR. **b** Densitometric data were normalized to β-actin in both types of cells. The bar graph represents the ratios of the expression of each gene in M-HPL1 (% of HPDL2). Data represent means ± SD (n=3)

The expression of various PDL-related genes was examined in cells from volunteer B and MFS1 patient by RT-PCR (Fig. 2c). Both types of PDL cells expressed *POSTN*, *ASPN*, *COL12A1*, *BGLAP*, *BSP*, and *COL1A1*. PDL cells from volunteer B expressed *OPN*. These results demonstrated that, induced by the culture conditions, the isolated PDL cells could differentiate into an osteoblastic phenotype.

Immortalization of isolated PDL cells

Since human cells have a limited life span (Sherr and DePinho 2000), and since the present PDL cells from the MFS1 patient with N2144S are valuable from a research viewpoint, the cultured cells (primary cells from volunteer B and MFS1 patient) were immortalized by retrovirus-mediated transduction. Non-transduced PDL cells and PDL cells transduced solely with *hTERT* showed senescence by passage 15. In contrast, PDL cells transduced with *Bmi-1* and *hTERT* did not show cellular senescence up to passage 20 as indicated by their cell morphology. Thus, we decided to transduce cells with both *Bmi-1* and *hTERT*. The transduced PDL cells from healthy volunteer B and the MFS1 patient were termed HPDL2 and M-HPL1, respectively.

Activation of telomerase by the transduction of *hTERT* was confirmed by the telomerase repeat amplification assay (Fig. 3a). Overexpression of Bmi-1 was confirmed by Western blot analysis (Fig. 3b). Bmi-1 was easily detected in M-HPL1 and HPDL2, but not in cells transduced solely with *hTERT*. No significant difference was seen in the cell growth between HPDL2 and M-HPL1 cultured in medium with 10% FBS up to day 15 (Fig. 3c). After day 12, the cell numbers of neither HPDL2 nor M-HPL1 increased extensively, suggesting that both types of cells had limited proliferation.

Phenotype of HPDL2 and M-HPL1

To characterize the phenotype of the immortalized PDL cells, expression of the reported PDL-related genes and β-actin was examined by semi-quantitative RT-PCR (Fig. 4a). HPDL2 and M-HPL1 both expressed *POSTN*, *ASPN*, *COL12A1*, *BGLAP*, *BSP*, and *COL1A1*. The relative expression of *POSTN*, *COL12A1*, *BGLAP*, and *COL1A1* was lower in M-HPL1 than in HPDL2 (Fig. 4b). *OPN* was expressed in HPDL2, but this was scarcely expressed in M-HPL1 (Fig. 4a, b). Immunohistochemistry with antibodies

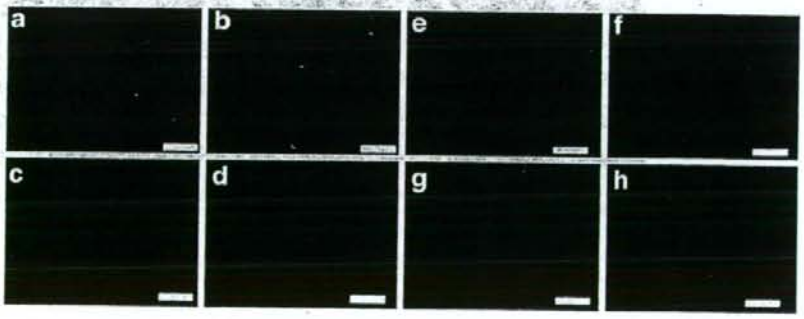

Fig. 5 Positive immunohistochemical localization of collagen type XII in cultured HPDL2 (**a**) and M-HPL1 (**b**) and of periostin in cultured HPDL2 (**e**) and M-HPL1 (**f**). Primary antibodies were replaced with mouse IgG (**c** HPDL2, **d** M-HPL1) or normal rabbit serum (**g** HPDL2, **h** M-HPL1) for negative controls. *Bars* 100 μm

against collagen type XII (Fig. 5a, b) and periostin (Fig. 5e, f) showed numerous immunostained cells in cultures of HPDL2 and M-HDL1. Staining was scarcely seen in negative controls in which primary antibodies had been replaced with mouse IgG (Fig. 5c, d) or normal rabbit serum (Fig. 5g, h).

In the lung (Neptune et al. 2003) and cardiovascular (Ng et al. 2004) systems, gene mutation in *FBN1* has been suggested to be involved in the activation of TGF-β. To examine whether this is the case in M-HPL1, immunostaining with LC1-30, which only recognizes the active form of TGF-β, was performed. M-HPL1 showed more intense staining than HPDL2 (Fig. 6e, f), although a comparable reaction was seen in HPDL2 and M-HPL1 to the antibody against LAP-β1, which also forms complexes with TGF-β (Fig. 6a, b; Miyazono et al. 1993). Staining was scarcely seen in negative controls, in which primary antibodies were replaced with normal goat serum (Fig. 6c, d) or normal rabbit serum (Fig. 6g, h).

Cell and fiber alignments in tissues transplanted with M-HPL1

Ectopic fiber formation by M-HPL1 and HPDL2 in the subcutaneous tissues of SCID mice was examined by transplantation of these cells with hydroxyapatite particles. In this experiment, hydroxyapatite was chosen because it is the major inorganic component of teeth and bones (Ten Cate 1998). HPDL2 (Fig. 7a) and M-HPL1 (Fig. 7b) both attached to the hydroxyapatite particles 18 h after being mixed with the particles.

Four weeks after the transplantation of the cells with hydroxyapatite particles into SCID mice, sections of the cells were immunostained with anti-vimentin antibody recognizing only human but not mouse cells. HPDL2 aligned in parallel between the particles (Fig. 8a, c). In contrast, M-HDL1 were

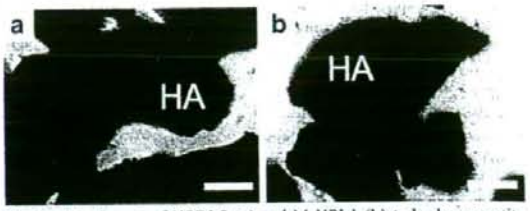

Fig. 7 Attachment of HPDL2 (**a**) and M-HPL1 (**b**) to hydroxyapatite particles (*HA*) after 18-h culture. *Bars* 100 μm

mainly located around the particles and were aligned irregularly (Fig. 8b, d). Similar observations were also seen in eight other transplants from a total of three SCID mice.

Transplanted tissues were immunostained with anti-human fibrillin-1 antibody. In contrast to the elaborate network of immunoreactive fibrillin-1 in HPDL2, M-HPL1 showed disorganized microfibril assembly (Fig. 9a, b). Staining was scarcely seen in the tissues in which the hydroxyapatite particles without cells were transplanted into SCID mice (Fig. 9c), demonstrating that the antibody only recognized human cells but not mouse cells.

Discussion

The present Japanese female patient had profound skeletal and cardiovascular symptoms including tall stature, arachnodactyly, aortic dissection, mitral valve prolapse, and severe periodontitis. Two types of Marfan syndrome (type I, MIM #154700; type II, MIM #154705) have been described so far. A large French family has been reported to exhibit the skeletal and cardiovascular features of Marfan syndrome in an autosomal dominant manner (Boileau et al. 1993). No mutation in *FBN1* has been seen in this family, and they have been classified as MFS2. Recently, *TGFBR2*

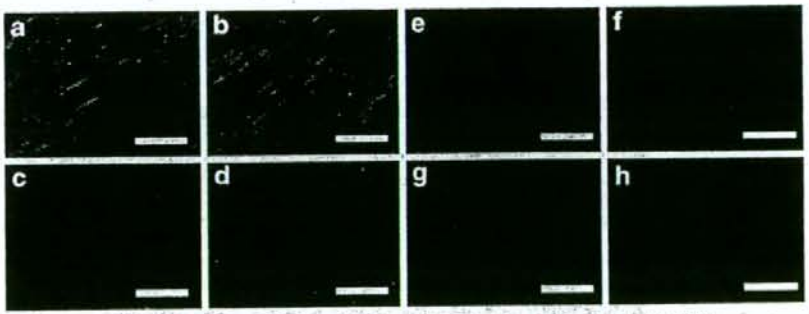

Fig. 6 Immunohistochemical localization of LAP-β1 in cultured HPDL2 (**a**) and M-HPL1 (**b**) and of LCI-30 in cultured HPDL2 (**e**) and M-HPL1 (**f**). Note that LCI-30, which recognizes only the active form of TGF-β, immunoreacts more abundantly in M-HPL1 than in HPDL2, whereas the level of LAP-β1 was comparable in the both types of cells. Primary antibodies were replaced with normal goat serum (**c** HPDL2, **d** M-HPL1) or normal rabbit serum (**g** HPDL2, **h** M-HPL1) for negative controls. *Bars* 100 μm

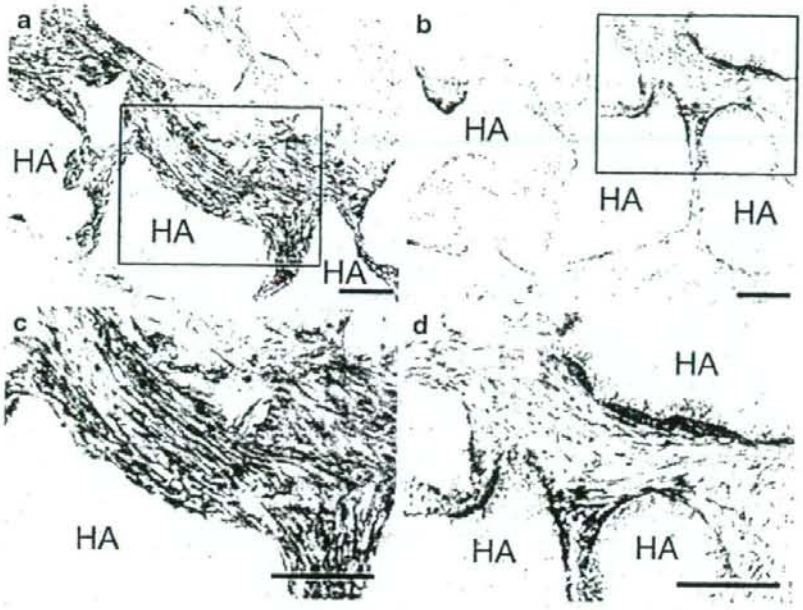

Fig. 8 Sections prepared from tissues in which HPDL2 (**a**, **c**) or M-HPL1 (**b**, **d**) were transplanted with hydroxyapatite particles (*HA*) into SCID mice for 4 weeks. Immunostaining with anti-human vimentin monoclonal antibody. The *boxed areas* in **a**, **b** are shown at higher magnification in **c**, **d**, respectively. Note that HPDL2 aligned in an organized manner, but M-HPL1 showed disorganized alignment. *Bars* 100 μm

has been identified as the responsible gene in MFS2 (Mizuguchi et al. 2004). The present patient has a heterozygous mutation in *FBN1* (Fig. 1f); this mutation results in a missense substitution (N2144S; Fig. 1g), clearly identifying the disease as MFS1.

Since *FBN1* is a large gene with 65 exons, direct sequencing of all the exons to identify mutations is time-consuming and costly. Therefore, we have performed DHPLC to screen for mutations in *FBN1*. In total, 65 amplicons for *FBN1* and 8 amplicons for *TGFBR2* have been synthesized by using specific primers by PCR. Heteroduplex formation has been identified in the product of exon 52 in *FBN1* by DHPLC (Fig. 1e). By using this method, systems have previously been developed to screen 20 congenital disorders (Kosaki et al. 2005). The present DHPLC method is a sensitive and powerful tool that allows the screening of gene mutations before direct sequencing; this is especially useful for large genes such as *FBN1*.

Cells isolated from the PDL of our MFS1 patient and of healthy volunteers have both shown increased ALP activity and mineralization in the cell differentiation medium. PDL cells are known to show an osteoblastic phenotype when cultured under these conditions (Cho et al. 1992; Giannopoulou and Cimasoni 1996; Nohutcu et al. 1997; Chien et al. 1999). After immortalization of cells by introducing *hTERT* and *Bmi-1*, both HPDL2 and M-HPL1 express PDL-related genes, viz., *POSTN* (Fujii et al. 2006), *ASPN* (Yamada et al. 2001), *COL12A1* (Fujii et al. 2006), *BGLAP* (Fujii et al. 2006), *BSP* (Yokoi et al. 2007), and *COL1A1* (Yokoi et al. 2007; Fig. 4a). These observations demonstrate that both types of cells have the characteristic phenotype of cultured PDL cells. However, *POSTN*, *COL12A1*, *BGLAP*, and *COL1A1*

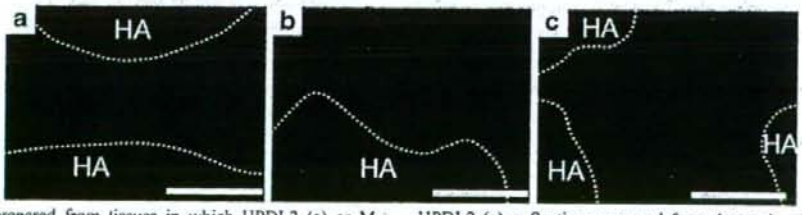

Fig. 9 Sections prepared from tissues in which HPDL2 (**a**) or M-HPL1 (**b**) were transplanted with hydroxyapatite particles (*HA*) into SCID mice for 4 weeks (*dotted lines* outline of HA). Immunostaining with anti-human fibrillin-1 antibody. Note the irregular microfibril assembly in the tissue implanted with M-HPL1 (**b**) but not in that with HPDL2 (**a**). **c** Sections prepared from tissues in which HA particles without cells were transplanted into SCID mice for 4 weeks. Note the absence of immunostaining with anti-human fibrillin-1 antibody (*dotted lines* outline of HA). *Bars* 50 μm

exhibit a lower expression in M-HPL1 than in HPDL2, and *OPN* is hardly expressed in M-HPL1 (Fig. 4a). We now need to examine whether PDL cells isolated from other MFS1 patients reveal a similar down-regulation of these genes.

Recently, attempts have been made to establish immortalized PDL cells by introducing *hTERT* (Berry et al. 2003; Kamata et al. 2004; Fujita et al. 2005; Saito et al. 2005; Fujii et al. 2006; Zhang et al. 2006). Cyclin-dependent kinase inhibitors $p16^{Ink4a}$ and $p21^{WAF1}$ induce premature senescence in human cells by telomere-independent mechanisms (Ramirez et al. 2001). As Bmi-1 can down-regulate the expression of $p16^{Ink4a}$ and $p14^{ARF}$ (Jacobs et al. 1999), it has been used to extend the life span of bovine and human cells (Dimri et al. 2002; Cudre-Mauroux et al. 2003; Itahana et al. 2003; Saito et al. 2005; Haga et al. 2007). Thus, in this study, we have immortalized human PDL cells with retrovirus-mediated transduction of both *hTERT* and *Bmi-1*. By using this method, both HPDL2 and M-HPL1 have been immortalized while maintaining their original gene expressions (Fig. 2c, Fig. 4a), as reported in cementoblast progenitor cells (Saito et al. 2005).

In MFS1, the activation of TGF-β signaling has been suggested as the pathogenesis for mitral valve prolapse and emphysema (Neptune et al. 2003; Ng et al. 2004). Mutations in *FBN1* alter or preclude matrix alteration of the latent complex of TGF-β, rendering TGF-β more accessible for activation (Neptune et al. 2003). In this study, activated TGF-β has been shown to be more abundant in M-HPL1 than in HPDL2 (Fig. 6e, f), suggesting that activated TGF-β signaling occurs in the PDL of our MFS1 patient.

N2144S in fibrillin-1 is predicted to alter one of the key calcium-binding residue ligands within the 32th cbEGF domain (Kettle et al. 1999; Yuan et al. 2002). This mutation is known to increase flexibility in the peptide backbone (Yuan et al. 2002). Attempts should be made to link this mutation and the disorganized cell alignment and microfibril assembly seen in this study.

OPN expression is lower in M-HPL1 than in HPDL2 (Fig. 4a). The exact reason for this difference is not known. However, TGF-β blockade has been reported significantly to enhance the BMP-2-induced upregulation of *OPN* expression, suggesting that TGF-β is a negative regulator on *OPN* expression (Shen et al. 2007). An examination is required of whether decreased expression of *OPN* (Fig. 4a) is mediated by the enhanced TGF-β activation in M-HPL1 (Fig. 6). Moreover, since no study has reported a relationship between fibrillin-1 and *OPN* expression, an investigation of *OPN* expression in M-HPL1 would be of interest after transfecting wild-type fibrillin-1 or during the culture of these cells on the fibrillin-1-coated dishes.

In summary, PDL cells have been isolated from an MFS1 patient with a heterozygous mutation in the 32th cbEGF domain (N2144S). These PDL cells have been immortalized by transducing human *mi-1* and *hTERT*. The present immortalized PDL cells show increased levels of activated TGF-β and should provide a powerful tool for the clarification of the biological roles of the elastic system fibers in PDLs and the pathogenesis of periodontitis in MFS1.

Acknowledgements The authors thank Dr. K. Ohyama (former Professor of Tokyo Medical and Dental University), Dr. S. Yamada (Osaka University), and Professor S. Murakami (Osaka University) for their valuable advice and discussion. The authors are also grateful to Professor T. Yoda (Saitama Medical University) and Dr. Y. Fukushima (Saitama Medical University) for organizing the tooth samples and providing the medical history of the patient. The authors also express their gratitude to Marfan Network Japan (MNJ) for their cooperation in the present research. Additional thanks are extended to Dr. T. Yokoi (Aichi Gakuin University), Dr. T. Tsubakimoto (Kanagawa Dental College), Dr. E. Nishida (Aichi Gakuin University), Dr. K. Kosaka (Kanagawa Dental College), and Dr. M. Aino (Aichi Gakuin University) for their technical assistance.

References

Bauss O, Sadat-Khonsari R, Fenske C, Engelke W, Schwestka-Polly R (2004) Temporomandibular joint dysfunction in Marfan syndrome. Oral Surg Oral Med Oral Pathol Oral Radiol Endod 97:592–598

Beertsen W, McCulloch CA, Sodek J (1997) The periodontal ligament: a unique, multifunctional connective tissue. Periodontol 2000:20–40

Berry JE, Zhao M, Jin Q, Foster BL, Viswanathan H, Somerman MJ (2003) Exploring the origins of cementoblasts and their trigger factors. Connect Tissue Res 44 (Suppl 1):97–102

Boileau C, Jondeau G, Babron MC, Coulon M, Alexandre JA, Sakai L, Melki J, Delorme G, Dubourg O, Bonaiti-Pellie C, Bourdarias JP, Junienet C (1993) Autosomal dominant Marfan-like connective-tissue disorder with aortic dilation and skeletal anomalies not linked to the fibrillin genes. Am J Hum Genet 53:46–54

Chien HH, Lin WL, Cho MI (1999) Interleukin-1beta-induced release of matrix proteins into culture media causes inhibition of mineralization of nodules formed by periodontal ligament cells in vitro. Calcif Tissue Int 64:402–413

Cho MI, Matsuda N, Lin WL, Moshier A, Ramakrishnan PR (1992) In vitro formation of mineralized nodules by periodontal ligament cells from the rat. Calcif Tissue Int 50:459–467

Cudre-Mauroux C, Occhiodoro T, Konig S, Salmon P, Bernheim L, Trono D (2003) Lentivector-mediated transfer of Bmi-1 and telomerase in muscle satellite cells yields a Duchenne myoblast cell line with long-term genotypic and phenotypic stability. Hum Gene Ther 14:1525–1533

Dietz HC, Cutting GR, Pyeritz RE, Maslen CL, Sakai LY, Corson GM, Puffenberger EG, Hamosh A, Nanthakumar EJ, Curristin SM, Stetten G, Meyers DA, Francomano CA (1991) Marfan syndrome caused by a recurrent de novo missense mutation in the fibrillin gene. Nature 352:337–339

Dimri GP, Martinez JL, Jacobs JJ, Keblusek P, Itahana K, Van Lohuizen M, Campisi J, Wazer DE, Band V (2002) The Bmi-1 oncogene induces telomerase activity and immortalizes human mammary epithelial cells. Cancer Res 62:4736–4745

Flanders KC, Thompson NL, Cissel DS, Van Obberghen-Schilling E, Baker CC, Kass ME, Ellingsworth LR, Roberts AB, Sporn MB (1989) Transforming growth factor-beta 1: histochemical local-

ization with antibodies to different epitopes. J Cell Biol 108: 653–660

Freeman E (1998) Periodontium. In: Ten Cate AR (ed) Oral histology: development, structure, and function, 5th edn. Mosby, St. Louis, pp 253–286

Fujii S, Maeda H, Wada N, Kano Y, Akamine A (2006) Establishing and characterizing human periodontal ligament fibroblasts immortalized by SV40T-antigen and hTERT gene transfer. Cell Tissue Res 324:117–125

Fujita T, Otsuka-Tanaka Y, Tahara H, Ide T, Abiko Y, Mega J (2005) Establishment of immortalized clonal cells derived from periodontal ligament cells by induction of the hTERT gene. J Oral Sci 47:177–184

Fullmer HM, Sheetz JH, Narkates AJ (1974) Oxytalan connective tissue fibers: a review. J Oral Pathol 3:291–316

Giannopoulou C, Cimasoni G (1996) Functional characteristics of gingival and periodontal ligament fibroblasts. J Dent Res 75: 895–902

Haga K, Ohno S, Yugawa T, Narisawa-Saito M, Fujita M, Sakamoto M, Galloway DA, Kiyono T (2007) Efficient immortalization of primary human cells by p16-specific short hairpin RNA or Bmi-1, combined with introduction of hTERT. Cancer Sci 98: 147–154

Handa K, Saito M, Yamauchi M, Kiyono T, Sato S, Teranaka T, Sampath Narayanan A (2002) Cementum matrix formation in vivo by cultured dental follicle cells. Bone 31:606–611

Hewett DR, Lynch JR, Smith R, Sykes BC (1993) A novel fibrillin mutation in the Marfan syndrome which could disrupt calcium binding of the epidermal growth factor-like module. Hum Mol Genet 2:475–477

Itahana K, Zou Y, Itahana Y, Martinez JL, Beausejour C, Jacobs JJ, Van Lohuizen M, Band V, Campisi J, Dimri GP (2003) Control of the replicative life span of human fibroblasts by p16 and the polycomb protein Bmi-1. Mol Cell Biol 23:389–401

Jacobs JJ, Kieboom K, Marino S, DePinho RA, Lohuizen M van (1999) The oncogene and Polycomb-group gene bmi-1 regulates cell proliferation and senescence through the ink4a locus. Nature 397:164–168

Kamata N, Fujimoto R, Tomonari M, Taki M, Nagayama M, Yasumoto S (2004) Immortalization of human dental papilla, dental pulp, periodontal ligament cells and gingival fibroblasts by telomerase reverse transcriptase. J Oral Pathol Med 33:417–423

Kapila YL, Kapila S, Johnson PW (1996) Fibronectin and fibronectin fragments modulate the expression of proteinases and proteinase inhibitors in human periodontal ligament cells. Matrix Biol 15:251–261

Kawamoto T, Shimizu M (2000) A method for preparing 2- to 50-micron-thick fresh-frozen sections of large samples and undecalcified hard tissues. Histochem Cell Biol 113:331–339

Kettle S, Yuan X, Grundy G, Knott V, Downing AK, Handford PA (1999) Defective calcium binding to fibrillin-1: consequence of an N2144S change for fibrillin-1 structure and function. J Mol Biol 285:1277–1287

Kielty CM, Sherratt MJ, Shuttleworth CA (2002) Elastic fibres. J Cell Sci 115:2817–2828

Kosaki K, Udaka T, Okuyama T (2005) DHPLC in clinical molecular diagnostic services. Mol Genet Metab 86:117–123

Kyo S, Nakamura M, Kiyono T, Maida Y, Kanaya T, Tanaka M, Yatabe N, Inoue M (2003) Successful immortalization of endometrial glandular cells with normal structural and functional characteristics. Am J Pathol 163:2259–2269

Maslen CL, Corson GM, Maddox BK, Glanville RW, Sakai LY (1991) Partial sequence of a candidate gene for the Marfan syndrome. Nature 352:334–337

Mecham RP (1991) Elastin synthesis and fiber assembly. Ann N Y Acad Sci 624:137–146

Miyazono K, Ichijo H, Heldin CH (1993) Transforming growth factor-beta: latent forms, binding proteins and receptors. Growth Factors 8:11–22

Mizuguchi T, Collod-Beroud G, Akiyama T, Abifadel M, Harada N, Morisaki T, Allard D, Varret M, Claustres M, Morisaki H, Ihara M, Kinoshita A, Yoshiura K, Junien C, Kajii T, Jondeau G, Ohta T, Kishino T, Furukawa Y, Nakamura Y, Niikawa N, Boileau C, Matsumoto N (2004) Heterozygous TGFBR2 mutations in Marfan syndrome. Nat Genet 36:855–860

Neptune ER, Frischmeyer PA, Arking DE, Myers L, Bunton TE, Gayraud B, Ramirez F, Sakai LY, Dietz HC (2003) Dysregulation of TGF-beta activation contributes to pathogenesis in Marfan syndrome. Nat Genet 33:407–411

Ng CM, Cheng A, Myers LA, Martinez-Murillo F, Jie C, Bedja D, Gabrielson KL, Hausladen JM, Mecham RP, Judge DP, Dietz HC (2004) TGF-beta-dependent pathogenesis of mitral valve prolapse in a mouse model of Marfan syndrome. J Clin Invest 114: 1586–1592

Nohutcu RM, McCauley LK, Koh AJ, Somerman MJ (1997) Expression of extracellular matrix proteins in human periodontal ligament cells during mineralization in vitro. J Periodontol 68:320–327

Nollen GJ, Mulder BJ (2004) What is new in the Marfan syndrome? Int J Cardiol 97 (Suppl 1):103–108

Pyeritz RE (2000) The Marfan syndrome. Annu Rev Med 51:481–510

Ramirez RD, Morales CP, Herbert BS, Rohde JM, Passons C, Shay JW, Wright WE (2001) Putative telomere-independent mechanisms of replicative aging reflect inadequate growth conditions. Genes Dev 15:398–403

Saito Y, Yoshizawa T, Takizawa F, Ikegame M, Ishibashi O, Okuda K, Hara K, Ishibashi K, Obinata M, Kawashima H (2002) A cell line with characteristics of the periodontal ligament fibroblasts is negatively regulated for mineralization and Runx2/Cbfa1/Osf2 activity, part of which can be overcome by bone morphogenetic protein-2. J Cell Sci 115:4191–4200

Saito M, Handa K, Kiyono T, Hattori S, Yokoi T, Tsubakimoto T, Harada H, Noguchi T, Toyoda M, Sato S, Teranaka T (2005) Immortalization of cementoblast progenitor cells with Bmi-1 and TERT. J Bone Miner Res 20:50–57

Sawada T, Sugawara Y, Asai T, Aida N, Yanagisawa T, Ohta K, Inoue S (2006) Immunohistochemical characterization of elastic system fibers in rat molar periodontal ligament. J Histochem Cytochem 54:1095–1103

Shen ZJ, Kim SK, Jun DY, Park W, Kim YH, Malter JS, Moon BJ (2007) Antisense targeting of TGF-beta1 augments BMP-induced upregulation of osteopontin, type I collagen and Cbfa1 in human Saos-2 cells. Exp Cell Res 313:1415–1425

Sherr CJ, DePinho RA (2000) Cellular senescence: mitotic clock or culture shock? Cell 102:407–410

Shiga M, Kapila YL, Zhang Q, Hayami T, Kapila S (2003) Ascorbic acid induces collagenase-1 in human periodontal ligament cells but not in MC3T3-E1 osteoblast-like cells: potential association between collagenase expression and changes in alkaline phosphatase phenotype. J Bone Miner Res 18:67–77

Staszyk C, Gasse H (2004) Oxytalan fibres in the periodontal ligament of equine molar cheek teeth. Anat Histol Embryol 33:17–22

Straub AM, Grahame R, Scully C, Tonetti MS (2002) Severe periodontitis in Marfan's syndrome: a case report. J Periodontol 73: 823–826

Ten Cate AR (1998) Hard tissue formation and destruction. In: Ten Cate AR (ed) Oral histology: development, structure, and function, 5th edn. Mosby, St. Louis, pp 69–77

Udaka T, Samejima H, Kosaki R, Kurosawa K, Okamoto N, Mizuno S, Makita Y, Numabe H, Toral JF, Takahashi T, Kosaki K (2005) Comprehensive screening of CREB-binding protein gene mutations among patients with Rubinstein-Taybi syndrome using

denaturing high-performance liquid chromatography. Congenit Anom 45:125–131

Westling L, Mohlin B, Bresin A (1998) Craniofacial manifestations in the Marfan syndrome: palatal dimensions and a comparative cephalometric analysis. J Craniofac Genet Dev Biol 18:211–218

Yamada S, Murakami S, Matoba R, Ozawa Y, Yokokoji T, Nakahira Y, Ikezawa K, Takayama S, Matsubara K, Okada H (2001) Expression profile of active genes in human periodontal ligament and isolation of PLAP-1, a novel SLRP family gene. Gene 275:279–286

Yokoi T, Saito M, Kiyono T, Iseki S, Kosaka K, Nishida E, Tsubakimoto T, Harada H, Eto K, Noguchi T, Teranaka T (2007) Establishment of immortalized dental follicle cells for generating periodontal ligament in vivo. Cell Tissue Res 327:301–311

Yuan X, Werner JM, Lack J, Knott V, Handford PA, Campbell ID, Downing AK (2002) Effects of the N2144S mutation on backbone dynamics of a TB-cbEGF domain pair from human fibrillin-1. J Mol Biol 316:113–125

Zhang X, Soda Y, Takahashi K, Bai Y, Mitsuru A, Igura K, Satoh H, Yamaguchi S, Tani K, Tojo A, Takahashi TA (2006) Successful immortalization of mesenchymal progenitor cells derived from human placenta and the differentiation abilities of immortalized cells. Biochem Biophys Res Commun 351:853–859

MOLECULAR AND CELLULAR BIOLOGY, Feb. 2008, p. 1338–1347 Vol. 28, No. 4
0270-7306/08/$08.00+0 doi:10.1128/MCB.01412-07

Regulation of MyD88-Dependent Signaling Events by S Nitrosylation Retards Toll-Like Receptor Signal Transduction and Initiation of Acute-Phase Immune Responses▽

Takeshi Into,[1]* Megumi Inomata,[1] Misako Nakashima,[1] Ken-ichiro Shibata,[2] Hans Häcker,[3] and Kenji Matsushita[1]

Department of Oral Disease Research, National Institute for Longevity Sciences, National Center for Geriatrics and Gerontology, 36-3, Gengo, Morioka, Obu, Aichi 474-8522, Japan[1]; Laboratory of Oral Molecular Microbiology, Department of Oral Pathobiological Science, Hokkaido University Graduate School of Dental Medicine, Sapporo 060-8586, Japan[2]; and Department of Infectious Diseases, St. Jude Children's Research Hospital, 332 North Lauderdale Street, Memphis, Tennessee 38105[3]

Received 7 August 2007/Returned for modification 23 September 2007/Accepted 28 November 2007

Nitric oxide (NO) has been thought to regulate the immune system through S nitrosylation of the transcriptional factor NF-κB. However, regulatory effects of NO on innate immune responses are unclear. Here, we report that NO has a capability to control Toll-like receptor-mediated signaling through S nitrosylation. We found that the adaptor protein MyD88 was primarily S nitrosylated, depending on the presence of endothelial NO synthase (eNOS). S nitrosylation at a particular cysteine residue within the TIR domain of MyD88 resulted in slight reduction of the NF-κB-activating property. This modification could be restored by the antioxidant glutathione. Through S nitrosylation, NO could negatively regulate the multiple steps of MyD88 functioning, including translocation to the cell membrane after LPS stimulation, interaction with TIRAP, binding to TRAF6, and induction of IκBα phosphorylation. Interestingly, glutathione could reversely neutralize such NO-derived effects. We also found that an acute febrile response to LPS was precipitated in eNOS-deficient mice, indicating that eNOS-derived NO exerts an initial suppressive effect on inflammatory processes. Thus, NO has a potential to retard induction of MyD88-dependent signaling events through the reversible and oxidative modification by NO, by which precipitous signaling reactions are relieved. Such an effect may reflect appropriate regulation of the acute-phase inflammatory responses in living organisms.

It is increasingly becoming evident that nitric oxide (NO) regulates a broad spectrum of protein functions through S nitrosylation, a posttranscriptional modification that forms *S*-nitrosothiol by covalent addition to cysteine residues of an NO moiety (14, 42, 43). Through S nitrosylation, NO is thought to exert a physiological inhibitory effect on nuclear factor κB (NF-κB) (25, 32, 33, 39), the major transcriptional factor family deeply associated with regulation of the immune system through transcription of a wide range of genes, including cytokines, adhesion molecules, antimicrobial molecules, and antiapoptotic molecules (10, 13, 24). S nitrosylation of NF-κB inhibits its DNA binding, promoter activity, and subsequent transcription (25, 33). It has been known that S nitrosylation targets a particular cysteine residue of the NF-κB p50 and p65 subunits located in the N-terminal DNA binding loop within the Rel homology domain (25, 32, 33). This residue is conserved in other NF-κB subunits, including p52, p100, p105, and c-Rel, and other Rel homology domain-containing molecules. Upstream of NF-κB, IκB kinase β (IKKβ), a catalytic subunit of the IκB (inhibitor of NF-κB) kinase complex, also undergoes S nitrosylation, resulting in reduction of its kinase function on phosphorylation of IκB (39). Such reduction of the IKKβ function leads to reduced IκB ubiquitinylation and proteasomal degradation, resulting in NF-κB inhibition (14, 32, 39).

Toll-like receptors (TLRs) are the central innate immune sensors for a broad array of pathogen-associated molecular patterns, ranging from bacterial constituents to viral genomes (2, 35). TLRs initiate early processes of proinflammatory immune responses that help to strengthen the processes of innate and adaptive immunity (2, 20), in which NF-κB plays many important roles (13, 24). TLRs utilize MyD88, a Toll/interleukin-1 receptor (IL-1R) homology (TIR) domain-containing adaptor molecule, to activate the NF-κB pathway through IL-1R-associated kinases (IRAKs) and tumor necrosis factor (TNF) receptor-associated factor 6 (TRAF6) (1). It has been thought that TLR agonistic molecules, such as lipopolysaccharide (LPS), can regulate NO generation through upregulation of expression of all NO synthase (NOS) isoforms through NF-κB activation (4, 9, 32). TLR stimulation can directly activate an antimicrobial property through inducible NOS (iNOS) expression and NO generation in macrophages (46). NO generation is a general feature of immune cells, including neutrophils, monocytes, macrophages, dendritic cells, and NK cells, as well as other cells, including endothelial cells, epithelial cells, and fibroblasts (4), all of which express multiple members of the TLR family. However, it has remained obscure whether generated NO exerts any regulatory effects on TLR signaling or subsequent processes of innate immune responses.

There has been an accumulation of biochemical evidence indicating that TLR signaling components, including IKKβ

* Corresponding author. Mailing address: Section of Oral Infection Control, Department of Oral Disease Research, National Institute for Longevity Sciences, National Center for Geriatrics and Gerontology, 36-3 Gengo, Morioka, Obu, Aichi 474-8522, Japan. Phone: 81-562-44-5651, ext. 5064. Fax: 81-562-46-8684. E-mail: into@nils.go.jp.

▽ Published ahead of print on 17 December 2007.

and NF-κB, might be regulated by S nitrosylation. S nitrosylation inhibits the kinase activity of apoptosis signal regulation kinase 1 (ASK1) through inhibition of its binding to substrates (38). ASK1 is known as an important regulator of the TRAF6-p38 mitogen-activated protein kinase (MAPK) pathway downstream of TLR4 and is also involved in modulation of both the NF-κB and apoptotic pathways downstream of TLR2 (19, 34). Caspse-1 was recently found to be involved in TLR2- and TLR4-mediated signal transduction of the MyD88-dependent pathway through the cleavage of the TIR domain-containing adaptor protein TIRAP (also known as Mal) (37). Caspase-1 also undergoes S nitrosylation at a cysteine residue within the enzymatic active site, suppressing its proteolytic activity (6, 31). Thus, it is possible that NO provides regulatory effects on the multiple steps of TLR-mediated innate immune signaling through S nitrosylation. In this study, we therefore designed experiments to determine the effect of S nitrosylation on TLR signaling. We further investigated how S nitrosylation affects TLR-initiated immune responses in vivo. We report here that S nitrosylation controls TLR signaling through redox-sensitive and reversible suppression of the MyD88 pathway, which facilitates appropriate control of acute-phase inflammatory responses in vivo.

MATERIALS AND METHODS

Reagents and cell culture. N^G-Monomethyl-L-arginine monoacetate (L-NMMA), *S*-nitrosoglutathione (GSNO), glutathione (GSH), *N*-ethylmaleimide, coumermycin A, *N*-acetyl L-cysteine (NAC), ascorbic acid, and diphenyleneiodonium (DPI) were obtained from Sigma-Aldrich. SNAP (5-nitroso-*N*-acetyl-D,L-penicillamine) was purchased from Cayman Chemical. ODQ (1*H*-[1,2,4]oxadiazolo[4,3-*a*]quinoxalin-1-one) and KT5823 were obtained from Calbiochem. Preparation of TLR ligands, including highly purified *Escherichia coli* LPS, *Salmonella* LPS, Pam_3CSK_4, macrophage-activating lipopeptide 2 (MALP-2), and *Salmonella enterica* serovar Typhimurium flagellin, was as described previously (18). Recombinant human IL-1β was from R&D Systems. Human aortic endothelial cells (HAECs) and human embryonic kidney 293 (HEK293) cells were maintained as described previously (18). HEK293 cells stably expressing human TLR4, MD2, and CD14 (293-TLR4 cells) and HEK293 cells stably expressing human TLR2 and CD14 (293-TLR2 cells) were obtained from InvivoGen.

Mice. iNOS-deficient ($iNOS^{-/-}$) mice and endothelial-NOS (eNOS)-deficient ($eNOS^{-/-}$) mice were from The Jackson Laboratories. C57BL/6J control (wild-type) mice were obtained from Japan SLC. All mice were kept under specific pathogen-free conditions. Male mice between 6 and 10 weeks of age were used for all of experiments. All animal protocols were approved by the National Institute for Longevity Sciences Animal Experimentation Committee at the National Center for Geriatrics and Gerontology (Aichi, Japan).

For LPS-induced acute lung injury, anesthetized mice received *Escherichia coli* LPS dissolved in pyrogen-free phosphate-buffered saline (PBS) containing 1 mg/ml Evans Blue intratracheally immediately after mechanical ventilation. After 30 min of administration, lung was excised and then lysed for immunoblot analysis. The febrile responses in mice treated with *E. coli* LPS were tested according to a protocol described previously (45, 49). Mice ($n = 6$) were maintained at a neutral ambient temperature of 31°C and challenged by intraperitoneal (i.p.) injection of 5 mg LPS/kg of body weight dissolved in pyrogen-free PBS. A high dose of LPS (more than 50 mg/kg) was fatal within 90 min in $eNOS^{-/-}$ mice. A colonic thermocouple was inserted and fixed to the base of the tail with adhesive tape. The change in temperature was monitored at 5-min intervals during a period of 120 min after LPS administration. All of the tests were performed at the temperature of 31°C. After 2 h or 12 h of LPS administration, 2 ml of PBS was injected into the abdominal cavity of each mouse. Then, fluids were collected and centrifuged for assessment of cytokine production by an enzyme-linked immunosorbent assay (ELISA). Preparation of peritoneal macrophages was as described previously (28).

Plasmids. The DNA construct encoding 3× Flag-tagged MyD88 fused to the B subunit of the bacterial DNA gyrase (MyD88-GyrB) was as described previously (11). Plasmids encoding human MyD88 and TIRAP were kind gifts from Margaret K. Offermann (Emory University School of Medicine). The cDNAs of N-terminal Flag-tagged and Myc-tagged MyD88, Myc-tagged TIRAP, IRAK-1 were amplified by PCR and cloned into the pcDNA3.1 vector (In gen). The construct encoding human TLR2 was as described previously Constructs encoding mutated Flag-MyD88 were obtained using a QuikCha site-directed mutagenesis kit (Stratagene) according to the manufacture structions.

Protein purification. Recombinant Flag-MyD88 proteins were prepared a FLAG M purification kit (Sigma-Aldrich) from HEK293 cells stably expr Flag-MyD88 constructs, according to the manufacturer's instructions. Pu recombinant proteins was confirmed by sodium dodecyl sulfate-polyacryl gel electrophoresis (SDS-PAGE), followed by silver staining and immun ting with anti-Flag antibody.

Detection of S-nitrosylated proteins. To detect S-nitrosylated MyD88 lung lysates from wild-type mice and $eNOS^{-/-}$ mice, we referred to the pr described by Jaffrey et al. (21). Several experiments were performed u NitroGlo nitrosylation detection kit (PerkinElmer) according to the ma turer's instructions. Lung lysates from wild-type and $eNOS^{-/-}$ mice wer jected to the biotin switching S-nitrosylation assay, and then biotinylated pr were purified on streptavidin-agarose. Purified proteins eluted by 2-mer ethanol were detected by immunoblotting with anti-MyD88 antibody.

The quantitative measurement of S-nitrosylated recombinant MyD ELISA was performed as follows. Briefly, recombinant Flag-MyD88 (15 was treated with or without SNAP for 30 min at 37°C in the dark. Then, th sulfides of Flag-MyD88 were blocked with 4 mM methylmethanethionsul for 15 min. After purification by using Micro Bio-Spin chromatography co (Bio-Rad Laboratories), Flag-MyD88 was reacted with 25 mM ascorbate completely denitrosylated. Free sulfides were then labeled with a biotin-gated maleimide, using a biotin labeling kit (SH; Dojindo Laboratories) a ing to the manufacturer's instructions. The diluents of biotinylated Flag-M proteins dissolved in Tris-buffered saline (pH 7.2) were stabilized in the w immobilizer streptavidin plates (Nunc). Flag-MyD88 proteins in the well detected by using anti-Flag antibody and a secondary antibody conjugate horseradish peroxidase. Colorimetric reaction was detected by absorbanc spectrophotometer at 450 nm. Results were expressed as means ± sta deviations (SD) of three determinations.

Photolysis of S-nitrosylated proteins. Mouse lung lysates were exposed min to a UV-visible light mercury vapor lamp according to a protocol re described (8). The samples were then subjected to the biotin switch techni described above.

Luciferase reporter assay. 293-TLR2 cells were transiently transfecte wild-type MyD88-GyrB or MyD88-GyrB mutants, each with a cysteine r replaced with a serine residue, together with 50 ng of an NF-κB (5×) luci reporter plasmid (pNF-κB-Luc; Stratagene) and 5 ng of an internal c luciferase reporter plasmid (pRL-TK; Promega) and incubated for 16 h. before the end of incubation, cells were treated with or without 250 μM Cells were then stimulated with 100 ng/ml Pam_3CSK_4 for 6 h. HEK29 stably expressing MyD88-GyrB were transfected with pNF-κB-Luc and pR After 24 h of incubation, cells were stimulated with coumermycin A presence and absence of 250 μM SNAP. The dual luciferase activity wa sured as described previously (19).

Immunoblot analysis of IRAK-1 and IκBα. HAECs were stimulated w ng/ml of LPS for 0 to 90 min. HEK293 cells stably expressing MyD88-GyrB stimulated with 1 μM coumermycin for 20 min. Cells were lysed in the pr of protease inhibitor and phosphatase inhibitor cocktails (Roche) at 4°C lysates or lysates from the mouse lungs were separated by SDS-PAGE, fo by immunoblot analyses using anti-IRAK-1, anti-IκBα, and phosphory specific anti-IκBα (Ser32/Ser36) antibodies (Cell Signaling Technology).

RNA extraction and reverse transcription-PCR. Total RNA was isolate mouse peritoneal macrophages stimulated with 100 ng/ml LPS and 10 gamma interferon, and transcripts were quantified by real-time quant reverse transcription-PCR on a LightCycler ST300 system (Roche). All were normalized to the level of β-actin mRNA. The primer sets used follows: for mouse macrophage inflammatory protein 2 (MIP-2), 5′-ATC AGCTTGAGTGTGACGC-3′ (sense) and 5′-AAGGCAAACTTTTTGA AA-3′ (antisense); for mouse IL-6, 5′-CCACGGCCTTCCCTAC-3′ (sens 5′-AGTGCATCATCGTTGTTC-3′ (antisense); and for mouse β-actin, ATCGTGCGTGACATCAAA-3′ (sense) and 5′-AAGGAAGGCTGGAA AGC-3′ (antisense).

Cytokine ELISA. Concentrations of human IL-8, mouse MIP-2, and IL-6 were determined using a Cytoset ELISA kit (Biosource) according manufacturer's instructions.

Subcellular fractionation. Subcellular fractionation of HEK293 cells expressing Flag-MyD88 and 293-TLR4 cells stably expressing Flag-MyD88

was performed using a ProteoExtract subcellular proteome extraction kit (Calbiochem) according to the manufacturer's instructions. This kit enables extraction of different subcellular fractions of the cytoplasm, plasma membrane, nuclei, and cytoskeleton from mammalian cells. 293-TLR4 cells stably expressing Flag-MyD88-GyrB were maintained in serum-free Dulbecco's modified Eagle's medium containing 5% PANEXIN H cell growth supplement (PAN Biotech GmbH) to avoid nonspecific cell activation by animal serum components. The whole-cell lysate was obtained using NuPAGE LDS sample buffer containing 2-mercaptoethanol. Each fraction was mixed with NuPAGE LDS sample buffer and boiled for 5 min, followed by SDS-PAGE and immunoblot analyses using anti-Flag (Sigma), anti-MyD88 (Santa Cruz Biotechnology), anti-IRAK-1, and anti-vimentin (BD Biosciences) antibodies.

Blue native PAGE and immunoprecipitation. HEK293 cells stably expressing Flag-MyD88 were treated with SNAP for 1 h, washed twice with PBS, and lysed with HEPES buffer (pH 7.2) containing 1% Triton X-100, 1% Nonidet-P40, and proteinase inhibitor cocktail (Roche). Cell lysates were separated by blue native PAGE according to the protocol provided by Invitrogen and then immunoblotted with anti-Flag antibody. HEK293 cells transiently transfected combinatorially with Flag-MyD88 and Myc-TIRAP or Flag-MyD88 and IRAK-1 were treated with GSNO or GSH for 1 h. HEK293 cells stably expressing 3× Flag-MyD88-GyrB were stimulated with 1 μM coumermycin A for 20 min. Cells were lysed with HEPES buffer (pH 7.2) containing 1% Triton X-100 and proteinase inhibitor cocktail (Roche). Clarified cell lysates were immunoprecipitated with anti-Flag antibody, followed by immunoblot analysis using anti-Flag, anti-Myc, and anti-TRAF6 (StressGen) antibodies. All experiments were performed at least three times, and representative results are shown.

Immunofluorescent cell staining. HAECs were fixed at −20°C with methanol, and double immunostaining was then carried out with anti-β-actin monoclonal antibody (Santa Cruz Biotechnology) and Alexa 488-conjugated immunoglobulin G secondary antibody (Invitrogen) and then with anti-MyD88 rabbit polyclonal antibody (Santa Cruz Biotechnology) and Alexa 564-conjugated immunoglobulin G secondary antibody (Invitrogen). Cell nuclei were also stained with 2.5 μg/ml of Hoechst 33342 for 30 min.

Statistical analysis. Probability (P) values were calculated by Student's t test and analysis of variance and were considered significant at 0.05 or 0.01.

RESULTS

TLR signaling components are S nitrosylated in vivo. To examine whether TLR signal components are physiologically S nitrosylated in vivo, we detected S-nitrosylated proteins in the lung lysates from wild-type and $eNOS^{-/-}$ mice by utilizing the biotin switch method (21). Interestingly, this method facilitated the detection of MyD88 as an S-nitrosylated protein (Fig. 1A). To exclude the possibility that the detection of S-nitrosylated MyD88 is an experimental artifact, we utilized the biotin switch method combined with photolysis of S nitrosylation, which has recently been reported as a useful method for confirming the specificity of S nitrosylation (8). The detectable S-nitrosylated MyD88 protein was reduced after exposure of the samples to a UV lamp (Fig. 1B), suggesting that the result is not false positive. Thus, our result at least suggests that MyD88 is potentially S nitrosylated in addition to other signaling molecules, including NF-κBs, ASK1, and caspase-1.

We further examined the details of S-nitrosylated MyD88 in vitro by utilizing a quantitative method for detecting S nitrosylation of recombinant proteins. We could detect S nitrosylation of recombinant MyD88, which increased, accompanied by an increase in the concentration of the NO donor SNAP (Fig. 1C). It has been known that S-nitrosylated proteins are reversibly denitrosylated by antioxidants or oxidoreductases, by which substantial protein functions are restored (14, 42). Indeed, the detectable S-nitrosylated MyD88 protein was reduced when the NO donor-treated protein was reacted with ascorbate, $HgCl_2$, or GSH (Fig. 1C). We further determined the site of S nitrosylation because the modification is effected toward particular cysteine residues (14). Mammalian MyD88 contains a total of nine cysteine residues: one in a short linker region and the other eight in the TIR domain (Fig. 1D). These residues are thought not to be involved in the formation of intramolecular disulfide bonds. Among vertebrates, all cysteine residues are highly conserved (data not shown). We prepared recombinant MyD88 proteins of nine individual mutants, each with one of the nine cysteine residues replaced with a serine residue. We found that the degrees of S nitrosylation of Cys113 and Cys216 were significantly reduced compared with those of wild-type MyD88 (Fig. 1E). These cysteine residues partially fulfill the predictive site of the S nitrosylation "acid-base motif" that comprises flanking acidic and basic residues (14) (Fig. 1F). Interestingly, the cysteine residue equivalent of Cys216 is conserved even in invertebrates, while others are not (data not shown). Among other TIR domain-containing adaptor molecules, only TIRAP and SIGIRR have a cysteine residue corresponding to the position of Cys216 (Fig. 1G).

To determine the requirement of cysteine residues for functioning of MyD88, we utilized MyD88 fused to the B subunit of the bacterial DNA gyrase (MyD88-GyrB). The *Streptomyces*-derived bivalent antibiotic coumermycin binds GyrB with a stoichiometry of 1:2, acting as a natural dimerizer of GyrB (7). Although overexpressed MyD88 is known to reveal TLR stimulation-independent nonspecific activation of downstream signaling through self-dimerization (11, 36), MyD88-GyrB does not reveal such nonspecific activation unless cells are exposed to TLR stimulation or coumermycin treatment (11). We prepared GyrB-fused wild-type MyD88 and MyD88 mutants, each with one of the nine cysteine residues replaced with a serine residue, and examined the NF-κB-activating properties in the TLR2 ligand Pam_3CSK_4-stimulated HEK293 cells stably expressing TLR2. None of the cysteine replacement mutants abrogated the NF-κB-activating property of MyD88 (Fig. 1H). However, the Cys216Ser mutant significantly increased the activity compared with that of wild-type MyD88 (Fig. 1H). Additionally, similar results were found in the cells treated with SNAP (Fig. 1H). Thus, it is possible that Cys216 of MyD88 mediates the suppressive effect of NO.

S nitrosylation alters MyD88-mediated signaling events. We next explored how S nitrosylation of signaling components alters TLR signaling events. To examine this in vivo, we utilized an animal model of acute lung injury induced by intratracheal administration of LPS. We investigated degradation of IRAK-1 and IκBα, hallmarks of MyD88-dependent and IKKβ-dependent signaling events, in the lungs 30 min after LPS administration. Interestingly, degradation of IRAK-1 and IκBα was apparently promoted in $eNOS^{-/-}$ mice compared with that in wild-type mice (Fig. 2A). We also examined whether NO alters degradation of IRAK-1 and IκBα in cultivated vascular endothelial cells. In HAECs, LPS induced degradation of IRAK-1 and IκBα within 30 min after stimulation (Fig. 2B). Degradation of IRAK-1 and IκBα was promoted and occurred within 15 min after stimulation when endogenous NO was predepleted by the L-arginine analog L-NMMA (Fig. 2B). In addition, IRAK-1 degradation was also promoted when confluent HAECs were maintained in culture media without the eNOS activator vascular endothelial growth factor or the phosphatidylinositol 3-kinase inhibitor LY294002 (data not shown). In contrast to these results, degradation was delayed

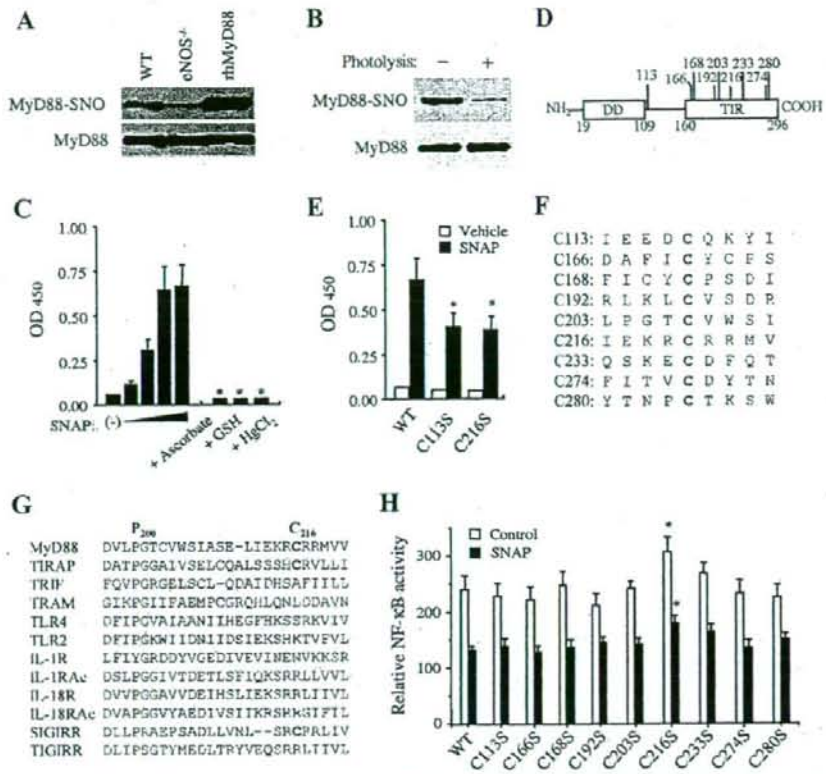

FIG. 1. S nitrosylaton of MyD88. (A) Lung lysates from wild-type (WT) and eNOS$^{-/-}$ mice and SNAP-treated recombinant human MyD (rhMyD88) were subjected to the biotin switching S-nitrosylation assay, and then biotinylated proteins were purified on streptavidin-agaro Purified proteins were detected by immunoblotting with anti-MyD88 antibody (upper). MyD88 proteins in lung lysates and rhMyD88 were a shown as loading controls (lower). (B) Mouse lung lysates were exposed for 3 min to a UV-visible light mercury vapor lamp. The samples w then subjected to the biotin switch method. (C) A recombinant Flag-MyD88 protein was treated with or without SNAP (100, 200, 500, and 1,(μM) for 30 min. For the denitrosylation study, SNAP-treated proteins were incubated with 1 mM ascorbic acid, 1 mM GSH, or 1 mM $HgCl_2$ 5 min before the blockade of free thiols by methylmethanethionsulfonate. Then, S-nitrosylated residues of MyD88 were switched into biot and proteins were fixed on streptavidin-coated plates, followed by ELISA with anti-Flag antibody. Each value is mean ± SD (n = 3). See text for details. (*, $P < 0.01$ for comparison with the group of 500 μM SNAP). (D) Schematic of human MyD (E) Recombinant Flag-MyD88 wild-type proteins and mutants with each cysteine residue replaced with a serine residue were treated with without 500 μM SNAP for 30 min. Then, S-nitrosylated MyD88 fixed on streptavidin-coated plates was detected by ELISA using anti-F antibody. Each value is the mean ± SD (n = 3). See text for details. (*, $P < 0.01$ for comparison with the wild-type group). (F) Sequence alignm of the region around nine cysteine residues of MyD88. (G) Sequence alignment of human TIR domain-containing molecules. The regi corresponding to that around the residues of Pro200, a critical residue for TIR-TIR interaction, and Cys216 of MyD88 are shown. (H) HEK2 cells stably expressing TLR2 were transiently transfected with GyrB-fused wild-type MyD88 or mutant MyD88 with each cysteine residue repla with a serine residue together with the NF-κB-driven luciferase gene and incubated for 16 h. At 6 h before the end of incubation, cells were trea with 200 μM SNAP. Cells were stimulated with 100 ng/ml Pam_3CSK_4 for 6 h, and then luciferase activity was measured. Each value is mean ± SD (n = 3). (*, $P < 0.05$ for comparison with the wild-type group).

and residual proteins were observed even at 45 min after stimulation when cells were pretreated with SNAP (Fig. 2B). The effect of NO was not altered in the presence of the guanylate cyclase inhibitor ODQ or the cyclic-GMP-dependent protein kinase inhibitor KT5823 (data not shown). Notably, LPS-induced degradation of IRAK-1 and IκBα in HAECs was prevented by the irreversible thiol modification by *N*-ethylmaleimide (Fig. 2C), implying that the effect of NO on the signaling events depends on modification of cysteine residues.

To test whether NO alters the MyD88-dependent signal events, we utilized the MyD88-GyrB construct. Under coumermycin treatment of cells stably expressing MyD88-GyrB, MyD GyrB undergoes dimerization and mimics TLR-triggered ty ical MyD88-dependent functions, such as the activation MAPKs and IKKs and secretion of proinflammatory cytoki (11). We found that coumermycin-dependent induction NF-κB activation in HEK293 cells was suppressed by pretre ment with cells with NO donors (Fig. 3A). Coumermycin co induce phosphorylation of IκBα at Ser32 and Ser36, the tar residues of IKKβ involved in degradation of IκBα (51), SNAP pretreatment could suppress induction of the respo (Fig. 3B). SNAP also suppressed coumermycin-induced ph

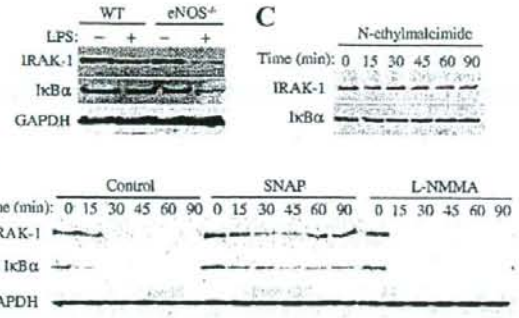

FIG. 2. NO suppresses LPS-induced degradation of IRAK-1 and IκBα. (A) Anesthetized wild-type (WT) and eNOS$^{-/-}$ mice intratracheally received *E. coli* LPS and mechanical ventilation. After 30 min of administration, lung was excised and then lysed for immunoblotting with anti-IRAK-1, anti-IκBα, and anti-GAPDH antibodies. (B) HAECs pretreated with 1 mM L-NMMA for 12 h or 0.25 mM SNAP for 1 h were stimulated with 10 ng/ml *E. coli* LPS for the indicated periods. The expression levels of IRAK-1 and IκBα were determined by immunoblot analysis. (C) HAECs pretreated with 0.1 mM *N*-ethylmaleimide for 10 min were stimulated with 10 ng/ml *E. coli* LPS for the indicated periods. The expression levels of IRAK-1 and IκBα were determined by immunoblot analysis.

phorylation of MAPKs (data not shown). The coumermycin-dependent dimerization of MyD88-GyrB induced interaction with TRAF6, consistent with a previous study (10), and we found that this interaction was reduced by SNAP treatment (Fig. 3C).

We found that NO and alteration of Cys113 and Cys216 residues of MyD88 did not alter the interaction of overexpressed MyD88 with IRAK-1 in HEK293 cells (Fig. 3D). However, NO clearly attenuated TLR4 stimulus (LPS)-dependent induction of MyD88–IRAK-1 interaction (Fig. 3E), suggesting that NO targets upstream signaling events of IRAK-1. It has been known that the recruitment of MyD88 to TLR2 or TLR4 is mediated by binding of the sorting adaptor TIRAP to the membrane phosphatidylinositol 4,5-bisphosphate, followed by interaction of MyD88 with TIRAP through TIR-TIR interaction (23). We examined whether NO affects the interaction of MyD88 with TIRAP. Overexpressed MyD88 interacted with TIRAP in HEK 293 cells (Fig. 3F). We found that treatment of the cells with the NO donor GSNO attenuated the interaction (Fig. 3F). We further investigated whether S nitrosylation of residues 113 and 216 is involved in MyD88-TIRAP interaction. Alteration of Cys residues did not affect the interaction (Fig. 3G). However, SNAP-induced attenuation of the interaction was reduced in the Cys216 mutant (Fig. 3G).

In HAECs, MyD88 was enriched with filamentous cytoskeletal structures and partly colocalized with β-actin (Fig. 4A). Additionally, a large part of MyD88 stably expressed in HEK293 cells was found in the cytoskeletal fraction (Fig. 4B). These findings are consistent with results of a previous study showing that MyD88 associates with β-actin in HeLa cells (22). Cytoskeletal MyD88 was separated from IRAK-1, which was found only in the cytoplasm (Fig. 4B), suggesting that MyD88 is maintained as an inactive state in cytoskeleton. We found that SNAP treatment altered such cytoskeletal localization of MyD88 into the cytoplasm (Fig. 4C). We further investigated the subcellular localization of MyD88 after TLR4 stimulation in 293-TLR4/MD2-CD14 cells stably expressing Flag-MyD88-GyrB. After LPS treatment, a part of MyD88 was transported to the cytoplasmic membrane from the cytoskeleton (Fig. 4D). However, SNAP treatment retarded such LPS-induced transportation of MyD88 (Fig. 4D). Although native PAGE analysis revealed that MyD88 formed a protein complex (more than 480 kDa) in HEK293 cells, SNAP treatment resulted in reduction in the size of the complex to approximately 450 kDa or 250 kDa, accompanied by an increase in concentration (Fig. 4E). Moreover, higher concentrations of SNAP further altered the complex to render a monomer (approximately 35 kDa) (Fig. 4E), implying disruption of functional MyD88 protein complex by NO.

Thus, NO has a capability to obstruct the MyD88 signing pathway through disruption of the multiple steps of protein interactions.

NO reversibly suppresses the MyD88 signaling events. S-nitrosylated proteins are known to undergo denitrosylation, by which regulatory effects of NO are conferred to control protein functions. We therefore investigated how S nitrosylation and denitrosylation affect MyD88-mediated signaling events. For this purpose, we utilized GSH because GSH had a capability to denitrosylate MyD88 (Fig. 1C). We found that GSH restored NO-induced impaired interaction of MyD88 with TIRAP (Fig. 4F). Furthermore, the NO-induced cytoplasmic localization of cytoskeletal MyD88 was restored by treatment of the cells with GSH (Fig. 4G). Thus, these results suggest that S nitrosylation alters the MyD88 pathway, and antioxidants or oxidoreductases restore such NO-derived actions, probably through denitrosylation.

NO reversibly suppresses TLR-mediated cellular responses. HAECs responded to multiple bacterial TLR agonistic molecules, Pam_3CSK_4 (for TLR1/TLR2), MALP-2 (for TLR2/TLR6), LPS (for TLR4), flagellin (for TLR5), and IL-1β, all of which are known to activate MyD88-dependnet signaling to induce production of the NF-κB-driven chemokine IL-8 after stimulation for 3 h (Fig. 5A). Predepletion of endogenous NO by L-NMMA resulted in a significant increase in IL-8 production induced by each stimulator (Fig. 5A), indicating that endogenous NO has a suppressive effect on the TLR-mediated cellular response. Furthermore, IL-8 production by each stimulator was suppressed in the presence of SNAP (Fig. 5A). The effect of NO donors was not altered in the presence of ODQ or KT5823 (data not shown). We investigated whether such a suppressive effect of NO can be restored because S nitrosylation is a reversible protein modification. However, it is difficult to examine the effects of antioxidants or oxidoreductases because the TLR signaling pathway is greatly affected by reactive oxygen species generated from NADPH oxidases (27, 34, 48). Indeed, treatment of cells with ascorbic acid, GSH, NAC, or the NADPH oxidase inhibitor DPI greatly impaired LPS-induced IL-8 production in HAECs (Fig. 5B). We therefore attempted to address whether the effect of NO is transient or persistent. For this purpose, HAECs were pretreated with SNAP for 1 h and washed two times to remove the NO donor. Then, at various times afterwards, the cells were stimulated with LPS and IL-8 production was measured. NO suppression of IL-8 production was gradually neutralized or restored in a